REPORT DOCUMENTATION PAGE

AFRL-SR-BL-TR-01-

0550

1. AGENCY USE ONLY (*Leave Blank*)	2. REPORT DATE	3. REPORT TYPE AND DATES COVERED
	October 4, 2001	Final Technical Report 01NOV98 – 31OCT00

4. TITLE AND SUBTITLE
Optical Fiber Gratings Using Near-UV Light

5. FUNDING NUMBERS
F49620-98-1-0051

6. AUTHORS
Jack Feinberg (Department of Physics)

7. PERFORMING ORGANIZATION NAME(S) AND ADDRESS(ES)
University of Southern California
Department of Contracts and Grants
Los Angeles, CA 90089-1147

8. PERFORMING ORGANIZATION REPORT NUMBER
Final Technical

9. SPONSORING / MONITORING AGENCY NAME(S) AND ADDRESS(ES)
Dr. Howard R. Schlossberg
AFOSR
801 N. Randolph Street, Room 732
Arlington, VA 22203-1977

10. SPONSORING / MONITORING AGENCY REPORT NUMBER

11. SUPPLEMENTARY NOTES

12a. DISTRIBUTION / AVAILABILITY STATEMENT
Unlimited

12b. DISTRIBUTION CODE

13. ABSTRACT (*Maximum 200 words*)

Experiments were performed to elucidate the physical mechanism by which light alters the refractive index of germanium-doped optical fibers. It was found that loading the fiber with hydrogen turns on a separate physical mechanism so that *all* of the Ge atoms become photosensitive and not just the Ge defects. New experimental results explain the reduced stability of optical fibers and fiber gratings in the presence of hydrogen, as well as the strength of gratings written through the polymer coating of optical fibers. A method is shown for writing long-period gratings in fibers with no unwanted harmonics or sidelobes. A new type of real-time fiber sensor is demonstrated that needs no spectrometer and senses either temperature or strain. In addition, a large number of specialty optical fiber gratings were fabricated in germanium-doped fibers and supplied to other research groups for demonstrations of systems applications including (a) adjustable dispersion compensators, (b) adjustable delay elements in a fiberoptic network, (c) mode-locked lasers that lase on multiple wavelengths, and (d) WDM systems that use packet headers.

14. SUBJECT TERMS
optical fibers
fiber gratings
fiber optic communications

15. NUMBER OF PAGES
25

16. PRICE CODE

17. SECURITY CLASSIFICATION OF REPORT	18. SECURITY CLASSIFICATION OF THIS PAGE	19. SECURITY CLASSIFICATION OF ABSTRACT	20. LIMITATION OF ABSTRACT
Unclassified	Unclassified	Unclassified	Unlimited

NSN 7540-01-280-5500

Standard Form 298 (Rev. 2-89)
Prescribed by ANSI Std. Z39-1
298-102

Final Report

F49620-98-1-0051

submitted to the
Air Force Office of Scientific Research
801 N. Randolph Street
Room 732
Arlington, VA22203-1977

ATTN: Dr. Howard Schlossberg

1) Date submitted: OCTOBER 4, 2001

2) Title: OPTICAL FIBER GRATINGS USING NEAR-UV LIGHT

3) Principal Investigator: JACK FEINBERG, DEPARTMENT OF PHYSICS
Office: (213) 740-1134, Fax: (213) 740-6653

4) Time period covered: 01 NOV 1998 – 31 OCT 2000

5) Institution Name: UNIVERSITY OF SOUTHERN CALIFORNIA, LOS ANGELES, CALIFORNIA 90089-0484

6) Federal agency identifying award number: F49630-98-1-0051

OPTICAL FIBER GRATINGS USING NEAR-UV LIGHT

F49630-98-1-0051

Jack Feinberg
Department of Physics
University of Southern California
Los Angeles, California 90089-0484
(213) 740-1134

A) Summary of Overall Progress:

1) We performed experiments to elucidate the physical mechanism by which light alters the refractive index of germanium-doped optical fibers. We found that loading the fiber with hydrogen turns on a separate physical mechanism so that *all* of the Ge atoms become photosensitive and not just the Ge defects.

2) We published new experimental results on the stability of optical fibers and fiber gratings in the presence of hydrogen.

3) We perfected ways of writing long-period gratings in fibers with no unwanted harmonics or sidelobes.

4) We performed experiments and presented new results on the strength of gratings written through the polymer coating of optical fibers.

5) We invented a new type of fiber sensor that needs no spectrometer and that works in real time. It senses either temperature or strain.

6) We fabricated a large number of fiber gratings in germanium-doped fibers and supplied these gratings to other research groups for demonstrations of systems applications. These include using fiber gratings (a) as adjustable dispersion compensators, (b) as adjustable delay elements in a fiberoptic network, (c) in mode-locked lasers that lase on multiple wavelengths, and (d) in WDM systems that use packet headers.

Details of these and other results are contained in the following publications and conference proceedings.

B) Publications and Conference Proceedings

Copies of selected papers from the publication list below are attached to this report.

PUBLICATIONS

1 "Group velocity dispersion cancellation and additive group delays by cascaded fiber Bragg gratings in Transmission," S. Wang, H, Erlig, H. Fetterman, E. Yablonovich, V. Grubsky, D. S. Starodubov, J, Feinberg, IEEE Microwave and Guided Wave Letters 8, 327-329 (1998)

2. "Ultrastrong fiber gratings and their applications," D. S. Starodubov, V. Grubsky, and J. Feinberg, Proceeding of the SPIE Vol. 3848, 178-185 (1999).

3. "Picosecond pulse generation at two wavelengths by simultaneous active mode locking in an Er-doped fiber laser with wide-bandwidth (>1 nm) nonchirped fiber Bragg gratings," O. Deparis, R. Kiyan, E. Salik, D. S. Staodubov, J. Feinberg, O. Pottiez, P. Megret, and M. Blondel, Proceedings of the SPIE, Vol 3847, 16-22 (1999).

4. "Photochemical reaction of hydrogen with germanosilicate glass initiated by 3.4 – 5.4 eV ultraviolet light," V. Grubsky, D. S. Starodubov, and J. Feinberg, Optics Letters 24, 729-731 (1999).

5. "Dynamic dispersion compensation in a 10-Gb/s optical system using a novel voltage tuned nonlinearly chirped fiber Bragg grating," K.-M. Feng, J.-X. Cai, V. Grubsky, D. W. Starodubov, M. I. Hayee, S. Lee, X. Jiang, A. E. Willner, and J. Feinberg, IEEE Photonics Technology Letters 11, 373-375 (1999).

6. "Fabrication of long-period fiber gratings with no harmonics," V. Grubsky, A. Skorucak, D. S. Starodubov, and J. Feinberg, IEEE Photonics Technology Letters 11, 87-89, (1999).

7. "Measurement of the temporal delay of a light pulse though a one-dimensional photonic crystal," S. Wang, H, Erlig, H. Fetterman, E. Yablonovich, V. Grubsky, D. S. Starodubov, J, Feinberg, Microwave and Optical Technology Letters 20, 17-21 (1999).

8. "Long-period fiber gratings with variable coupling for real-time sensing application," V. Grubsky and J. Feinberg, Optics Letters 25, 203-205 (2000).

9. "All fiber WDM Optical Crossconnect using Ultrastrong widely tunable FGS," Y.W. Song, Z. Pan, D. Starodubov, V. Grubsky, E. Salik, S.A. Havstad, Y. Xie, A. E. Willner, and J. Feinbeg, IEEE Photonics Technology Letters, 13, 1103-1105 (2001).

CONFERENCE PROCEEDINGS

10. "Fabrication of spectrally clean, long-period grating filters," V. Grubsky, A. Skorucak, J. Feinberg, and D. S. Starodubov, Optical Fiber Communication Conference OFC'99, San Diego, California February 21-26 (1999).

11. "Sampled nonlinearly chirped fiber Bragg grating for the tunable dispersion compensation of many WDM channels simultaneously, "J.-X. Cai, K. M. Feng, A. E. Willner, V. Grubsky, D. S. Starodubov, J. Feinberg, Optical Fiber Communication Conference OFC'99, San Diego, California February 21-26 (1999).

12. "All-optical packet header recognition and switching in a reconfigurable network using fiber Bragg gratings for time-to-wavelength mapping and decoding," M. C. Cardakli, S. Lee, A. E. Willner, V. Grubsky, D. S. Starodubov, and J. Feinberg, Optical Fiber Communication Conference OFC'99, San Diego, California February 21-26 (1999).

13. "All-fiber bandpass filter with adjustable transmission," D. S. Starodubov, V. Grubsky, and J. Feinberg, Optical Fiber Communication Conference OFC'99, San Diego, California February 21-26 (1999).

14. "Thermally stable gratings in optical fibers without temperature annealing," E. Salik, D. S. Starodubov, V. Grubsky, and J. Feinberg, Optical Fiber Communication Conference OFC'99, San Diego, California February 21-26 (1999).

15. "Effect of molecular water on thermal stability of gratings in hydrogen-loaded optical fibers," V. Grubsky, J. Feinberg, and D. S. Starodubov, Optical Fiber Communication Conference OFC'99, San Diego, California February 21-26 (1999).

16. "High-birefringence nonlinearly-chirped fiber Bragg grating for tunable compensation of polarization-mode dispersion," S. Lee, R. Khosravani, A.

E. Willner, V. Grubsky, D. S. Starodubov, J. Feinberg, and J. Peng, Optical Fiber Communication Conference OFC'99, San Diego, California February 21-26 (1999).

17. "Control monitoring of routing bits and data packets in WDM networks using wavelength-to-time mapping," X. Jiang, M. Carkakli, K. M. Feng, J. X. Cai, A. E. Willner, V. Grubsky, D. S. Starodubov, and J. Feinberg, Optical Fiber Communication Conference OFC'99, San Diego, California February 21-26 (1999).

18. "Fiber Bragg gratings for diode lasers," at the 1999 Diode Laser Technology Review, Ft. Walton Beach, Florida, May 11-13 (1999).

19. "Optical fiber gratings: New fabrication techniques and components," D. S. Starodubov, V. Grubsky, and J. Feinberg, LEOS Summer Topical Meeting on WDM Components, San Diego, CA, July 26-30 (1999).

20. "Fiber Bragg grating technology," J. Feinberg and D. S. Starodubov (invited tutorial), OSA Annual Meeting, Santa Clara, CA Sept 26 - Oct 1 (1999).

21. "Long-period grating fiber sensor with fixed resonance wavelength," V. Grubsky and J. Feinberg, OSA Topical Meeting on Bragg Gratings, Photosensitivity, and Poling in Glass Waveguides, Stuart Florida, September 23-25 (1999).

22. "Novel fiber radiation sensor using long-period gratings, A. Skorucak, D. S. Starodubov, and J. Feinberg, OSA Topical Meeting on Bragg Gratings, Photosensitivity, and Poling in Glass Waveguides, Stuart Florida, September 23-25 (1999).

23. "The role of oxygen deficient centers in hydrogen-loaded germanosilicate glass," D. S. Starodubov, V. Grubsky, M. Ewart, J. Feinberg, E. M. Dianov, A. A. Rybaltovskii, and A. O. Rybaltovskii," OSA Topical Meeting on Bragg Gratings, Photosensitivity, and Poling in Glass Waveguides, Stuart Florida, September 23-25 (1999).

24. "Ultrastrong fiber gratings and their applications," D. S. Starodubov, V. Grubsky, and J. Feinberg, Proceeding of the SPIE Meeting on Optical Fiber Reliability and Testing, Boston, Massachusetts, September 20-21 (1999).

25. "Picosecond pulse generation at two wavelengths by simultaneous active mode locking in an Er-doped fiber laser with wide-bandwidth (>1 nm) nonchirped fiber Bragg gratings," O. Deparis, R. Kiyan, E. Salik, D. S. Staodubov, J. Feinberg, O. Pottiez, P. Megret, and M. Blondel, SPIE Meeting on Optical Devices for Fiber Communication, Boston, Massuchusetts, September 20-21 (1999).

C) Current Problems or Unusual Developments:

None.

D) Changes from Original Proposal:

None.

E) Personnel Supported

Jack Feinberg, principal investigator

Anton Skorucak, graduate student

Ertan Salik, graduate student

F) Interactions

Prof. Howard Fetterman, Dept. of Electrical Engineering, UCLA

Prof. Alan E. Willner, Dept. of Electrical Engineering-Systems, USC

Prof. Olivier Duparis, Faculté Polytechnique de Mons, Belgium

Prof. E. M., Dianov, Fiber Optics Research Center, General Physics Institute, Moscow, Russia

G) New Discoveries, Inventions, or Patent Disclosures

"Optical Fiber Grating Sensor with Fixed Wavelength." publicly disclosed August, 1999. Patent disclosure filed with USC but USC declined filing a patent application.

H) Honors or Awards

None.

Group Velocity Dispersion Cancellation and Additive Group Delays by Cascaded Fiber Bragg Gratings in Transmission

Shamino Wang, *Student Member, IEEE,* Hernan Erlig, *Student Member, IEEE,* Harold R. Fetterman, *Fellow, IEEE,* Eli Yablonovitch, *Fellow, IEEE,* Victor Grubsky, Dmitry S. Starodubov, and Jack Feinberg

Abstract— **We have demonstrated that cascaded fiber Bragg gratings can provide delays of propagating pulses with minimal pulse reshaping. The grating pair used exhibited an overlap transmission region centered at 1551.05 nm, where both gratings contribute to the group delay and the group velocity dispersion (GVD) was canceled. Using wavelength tunable pulses spectrally sliced from a mode-locked fiber laser, the measurement was performed in the time domain with single picosecond resolution. Both gratings were 3 mm long and a maximum group delay of 15 ps was measured for the cascaded sequence. This compound grating configuration can be implemented as encoders and decoders in spread spectrum CDMA systems.**

Index Terms— **CDMA, dispersion compensation, fiber Bragg grating, group delay, wavelength slicing.**

I. Introduction

UNIFORM fiber Bragg gratings, essentially one-dimensional photonic crystals, exhibit low group velocity and large dispersion near their stop bands. Therefore, delays can be achieved in transmission at band edge frequencies of uniform gratings, eliminating the need for circulators or couplers in conventional reflection schemes [1]. These delays are also coupled with dispersion, which severely limits their application to communication systems. In this letter we demonstrate that this dispersion can be effectively compensated for by transmission through opposite sides of grating pair stop bands, while both gratings contribute to the additive delay. Simulations have demonstrated the advantages afforded by gratings in long-haul fiber dispersion compensation [2], [3]. So far experimental investigations in this arena have been performed in the frequency domain [4] or in the time domain using a 50-GHz sampling oscilloscope [5]. Previously we reported single picosecond resolution time-domain measurements of group delay incurred by optical pulses propagating through a uniform grating [6]. We also demonstrated that the group delay was additive for nearly identical cascaded gratings; however, the transmitted pulse was severely distorted [7].

In this letter we explore a fiber Bragg grating pair that provided a 15-ps group delay with compensated GVD in transmission. The gratings were 3 mm long each and spatially separated to avoid any coupling effect. The measured transmission spectrum is shown in Fig. 1. The grating pair exhibited bandgap centers at 1550.25 and 1552.10 nm with 3-dB bandwidths of 1.40 and 1.82 nm, respectively. The overlap transmission region had a 1551.05-nm central wavelength, a 0.5-nm 3-dB bandwidth, and −3-dB peak intensity transmission. A commercial simulation program was used to model the gratings with parameters chosen to match the measured transmission spectrum. The simulated group velocities are shown in Fig. 2. The constant effective group velocity from 1550.99 to 1551.10 nm in the overlap transmission region resulted from GVD and higher order dispersion compensation. This was confirmed experimentally in the time domain by the minimal pulse distortion.

II. Experimental Setup

The output from a 1.55-μm mode-locked erbium-doped fiber laser exhibiting a 56-nm bandwidth was spectrally sliced [8] by an HP optical spectrum analyzer. The resulting 0.5-nm bandwidth pulses produced a ~16-ps full-width at half-maximum (FWHM) auto-correlation. Using a 3-dB coupler the pulse train was divided into the grating pair and into a reference fiber, subsequently recombined, and fed to an auto-correlator. The pulse train timing difference was then measured from the separation between the cross-correlation and auto-correlation traces, and the grating pair induced pulse distortion from the cross-correlation trace, by varying the center frequency of the 0.5-nm optical pulses. This experimental arrangement was detailed in [6] and [7].

III. Results

The wavelengths at which the measurements were performed are labeled on the transmission spectrum. Point A was situated at 1545.00 nm where we expected no grating pair effect. E was at the center of the overlap transmission region. B and F were on opposite sides of the spectrum and had the same transmission as E. D produced the same delay as that of E. C was the spectral midpoint of B and D.

For some of these wavelengths the correlation traces are plotted in Fig. 3(a). The 52-ps separation between the cross-

Manuscript received April 27, 1998. This work was supported by the Air Force Office of Scientific Research (AFOSR) and by the Ballistic Missile Defense Organization (BMDO).

S. Wang, H. Erlig, H. R. Fetterman, and E. Yablonovitch are with the Electrical Engineering Department, University of California, Los Angeles, CA 90095 USA.

V. Grubsky, D. S. Starodubov, and J. Feinberg are with the Physics Department, University of Southern California, Los Angeles, CA 90089-0484 USA.

Publisher Item Identifier S 1051-8207(98)08535-3.

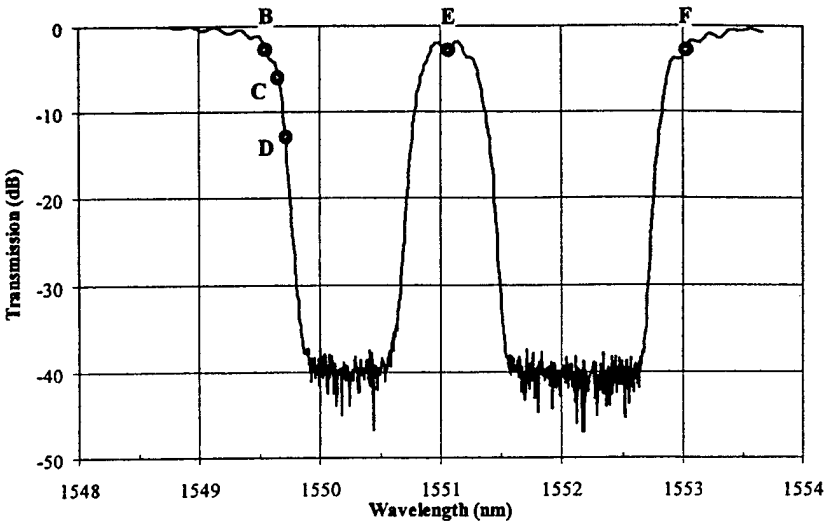

Fig. 1. Transmission spectrum of the grating pair, with bandgap centers at 1550.25 and 1552.10 nm, and 3-dB bandwidths 1.40 and 1.82 nm, respectively. The overlap transmission region had a 1551.05-nm central wavelength, a 0.5-nm 3-dB bandwidth, and −3-dB peak intensity transmission. Operating wavelengths of interest are B: 1549.55 nm, C: 1549.63 nm, D: 1549.70 nm, E: 1551.05 nm, and F: 1553.01 nm.

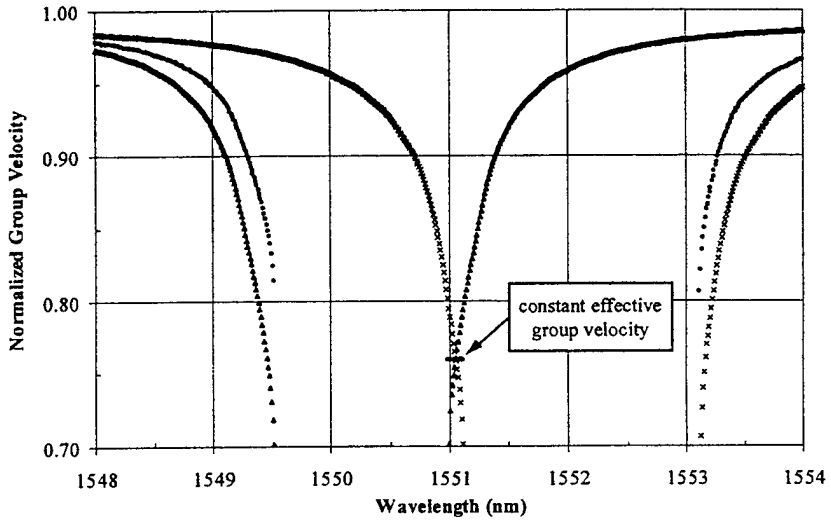

Fig. 2. IFO_Gratings simulation results. (△) normalized group velocity of the grating centered at 1550.25 nm, (×) normalized group velocity of the grating centered at 1552.10 nm, and (•) normalized effective group velocity of the gratings cascaded. The group velocities are normalized to the speed of light in bare fiber. Note the almost flat effective group velocity from 1550.99 to 1551.10 nm.

correlation and auto-correlation traces for point A was intentionally introduced by choosing the grating pair arm ~1 cm longer. Group delays of 11, 13, 15, 15, and 7 ps for points B, C, D, E, and F, respectively, were measured as the additional displacement of the cross-correlation trace relative to the auto-correlation trace. The maximum 15-ps delay corresponds to a group velocity 66% of the speed of light in bare fiber. Assuming a symmetric bandgap for each of the gratings the delay at E was expected to equal that at B plus F, 18 ps. At points E, B, and F the transmission loss amounted to 3 dB. In comparison, point D provided the same delay as E with a 13-dB transmission loss.

A zoom-in view of the cross-correlation traces for several wavelengths is shown in Fig. 3(b). From these we deduced the extent of pulse reshaping. The traces were purposefully superimposed and normalized to their respective peak values for ease of comparison. The structure that appeared at ~90 ps was caused by the leading edge of the auto-correlation trace. The cross-correlation at A exhibited a FWHM of 19.0 ps and it was taken as the reference pulse shape. Operation at E produced a cross-correlation trace with a FWHM of 21.5 ps, 13% larger than that at A. There were three reasons for the slight pulse reshaping at E. First, for a uniform grating, there were oscillations in the transmission and group velocity characteristics [4]. Second, although the GVD was canceled, cubic and higher order dispersion were not [2]. Third, the 0.5-nm pulse bandwidth was larger than the 0.11-nm zero dispersion region. At C and D the cross-correlation FWHM were 28.3 and 29.3 ps, respectively. The pulses widened as expected since at these points there was no dispersion compensation.

IV. Conclusion

We have experimentally demonstrated a grating pair sequence with wavelength dependent group delay exhibiting

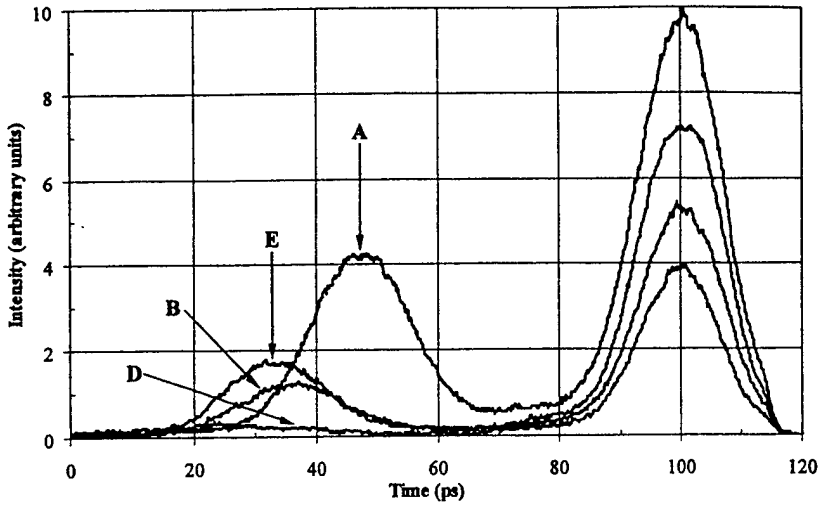

(a)

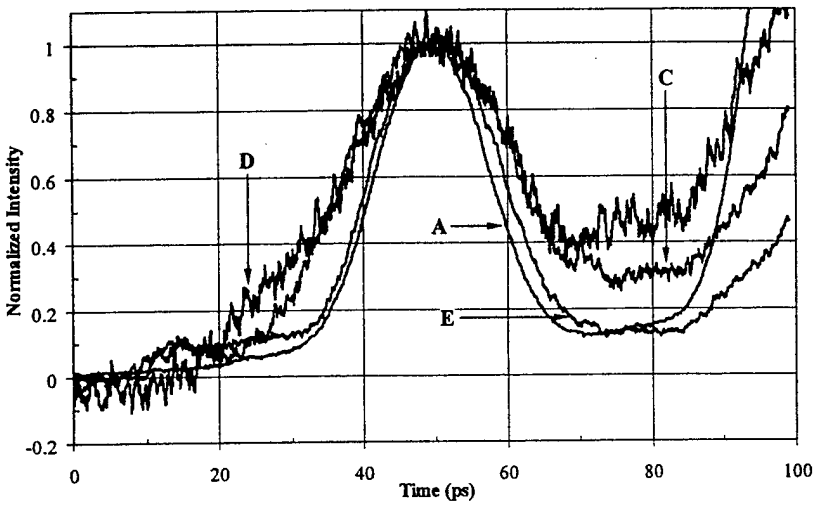

(b)

Fig. 3. (a) Correlation traces for the various operating wavelengths. The auto-correlation traces are located at 100 ps. (b) Zoom-in view of normalized cross-correlation traces for various operating wavelengths defined in Fig. 1.

compensated GVD over a 0.5-nm band. Over this range both gratings contributed to the optical pulse propagation characteristics enabling a 15-ps group delay with 3-dB transmission loss. One possible application of this is in matched filtering schemes, where for a fixed center wavelength one grating in the transmitter stretches the pulse in time while a conjugate grating in the receiver is used for pulse reconstruction. Both gratings can be further expanded as specially designed grating sequences to meet orthogonal code requirements among different channels for CDMA systems.

ACKNOWLEDGMENT

The authors would like to thank Prof. B. Jalali's group for support with the optical instrumentation.

REFERENCES

[1] W. H. Loh, R. I. Laming, N. Robinson, A. Cavaciuiti, F. Vaninetti, C. J. Anderson, M. N. Zervas, and M. J. Cole, "Dispersion compensation over distances in excess of 500 km for 10-Gb/s systems using chirped fiber gratings," *IEEE Photon. Technol. Lett.*, vol. 8, pp. 944–946, July 1996.

[2] N. M. Litchinitser, B. J. Eggleton, and D. B. Patterson, "Fiber Bragg gratings for dispersion compensation in transmission: Theoretical model and design criteria for nearly ideal pulse recompression," *J. Lightwave Technol.*, vol. 15, pp. 1303–1313, Aug. 1997.

[3] N. M. Litchinitser and D. B. Patterson, "Analysis of fiber Bragg gratings for dispersion compensation in reflective and transmissive geometries," *J. Lightwave Technol.*, vol. 15, pp. 1323–1328, Aug. 1997.

[4] B. J. Eggleton, T. Stephens, P. A. Krug, G. Dhosi, Z. Brodzeli, and F. Ouellette, "Dispersion compensation using a fiber grating in transmission," *Electron. Lett.*, vol. 32, pp. 1610–1611, Aug. 1996.

[5] B. J. Eggleton, C. M. de Sterke, and R. E. Slusher, "Nonlinear pulse propagation in Bragg gratings," *J. Opt. Soc. Amer. B*, vol. 14, pp. 2980–2993, Nov. 1997.

[6] S. Wang, H. Erlig, H. R. Fetterman, E. Yablonovitch, V. Grubsky, D. S. Starodubov, and J. Feinberg, "Measurement of the temporal delay of a light pulse through a one-dimensional photonic crystal," *Microwave Opt. Technol. Lett.*

[7] S. Wang, H. Erlig, H. R. Fetterman, V. Grubsky, and J. Feinberg, "One-dimensional photonic crystals for CDMA," in *Multimedia Networks: Security, Displays, Terminals, and Gateways, Proc. SPIE 3228*, 1997, pp. 408–417.

[8] T. M. Goyette, W. Guo, F. C. De Lucia, J. C. Swartz, H. O. Everitt, B. D. Guenther, and E. R. Brown, "Femtosecond demodulation source for high-resolution submillimeter spectroscopy," *Appl. Phys. Lett.*, vol. 67, pp. 3810–3812, Dec. 1995.

Photochemical reaction of hydrogen with germanosilicate glass initiated by 3.4–5.4-eV ultraviolet light

V. Grubsky, D. S. Starodubov, and J. Feinberg

Department of Physics, University of Southern California, Los Angeles, California 90089-0484, and D-STAR Technologies, Inc., 725 33rd Street, Manhattan Beach, California, 90266

Received February 10, 1999

By measuring the photosensitivity of Ge-doped silica fibers over the 3.4–5.4-eV spectral range and from $T = 95$ K to $T = 375$ K, we demonstrate that different physical mechanisms take place depending on whether H_2 is present. Without H_2 the principal photosensitivity pathway involves excitation of a germanium oxygen-deficient center to its triplet state. In H_2-loaded fibers the UV light excites the regular Ge—O bond, which then reacts with H_2 to produce Si—OH or Ge—OH and a GeE′ center. © 1999 Optical Society of America

OCIS codes: 060.2290, 060.2400, 050.2770.

To make its fiber gratings the telecommunications industry depends on the photosensitivity of Ge-doped silica fibers.[1] In such fibers UV light causes a change in the refractive index of the glass. With no H_2 in the fiber, the photosensitivity has been ascribed to germanium oxygen-deficient centers (GODC's), which can be excited through their absorption bands at 240 nm (Ref. 1) or 330 nm.[2] However, if H_2 is present the physics alters dramatically.

In this Letter we analyze the spectrum of photosensitivity of germanosilicate fibers both with and without H_2. We were able to measure the photosensitive response over a broad range of UV photon energies, from 3.41 eV (364 nm) to 5.41 eV (229 nm). For H_2-loaded fibers we investigated the change of the photosensitivity spectrum with temperature. We also measured the spectrum and magnitude of the induced OH absorption, and we show that the magnitude correlates with the measured refractive-index change. Based on these data, we propose a mechanism that explains the UV-induced reaction of H_2 with glass and is in good agreement with the previous experiments discussed below.

Lemaire *et al.* showed that the response of germanosilicate fibers to UV light could be enhanced by two orders of magnitude by use of high-pressure H_2 loading before writing.[3] After irradiating H_2-loaded fibers with pulsed 241-nm light, they observed a large refractive-index change ($\Delta n \sim 3 \times 10^{-3}$) and a large concentration (~8 mol. %) of induced OH, which was roughly twice the initial concentration of H_2. The authors suggested that the index change was caused by a reaction of H_2 at normal Ge sites to produce OH groups and oxygen-deficient centers. Atkins *et al.*[4] reported that UV irradiation of H_2-loaded fibers caused almost complete bleaching of the 240-nm absorption band of the GODC and induced strong absorption at ~205 nm (possibly owing to GeE′ centers) and shorter wavelengths. The induced absorption continued to grow long after the GODC band was bleached. Albert *et al.*[5] produced an index change in H_2-loaded Ge-doped glass that had no GODC's (no initial absorption band at 240 nm); they used 193- and 248-nm light as sources of UV radiation. Tsai *et al.*[6] observed efficient generation of GeE′ centers (• Ge≡) with UV irradiation of H_2-loaded fibers compared with unloaded fibers. Finally, Lemaire *et al.*[7] showed that heating H_2-loaded glass to 250–400 °C increased its photosensitivity, which was attributed to an increase of UV absorption at elevated temperature, thereby increasing the excitation of Ge—O bonds.

There have been a few attempts to produce an index change in H_2-loaded glass by use of light of wavelength longer than 248 nm. Martin and Ouelette fabricated strong gratings in H_2-loaded fibers by use of 266-nm light.[8] Atkins and Espindola attempted to write Bragg gratings with 325- and 351-nm light but succeeded in making only a weak and unstable grating.[9] Using 334-nm light, we demonstrated efficient fabrication of stable Bragg gratings in H_2-loaded fibers,[10] and with permanent index changes as large as $\Delta n = 1.1 \times 10^{-2}$ (Ref. 11), which is comparable with Δn produced at 240 nm. We also demonstrated that the rate of the index change in H_2-loaded fibers was proportional to the Ge concentration in the fiber.[11]

Here we present results of new experiments to measure the photosensitivity of Ge-doped fiber both with and without H_2. We used mostly 10-mol. % Ge-doped fiber and nine laser lines spanning the spectral range from 229 nm (from a Lexel frequency-doubled argon laser) to 364 nm (from a Coherent UV argon laser).

To load the fibers with H_2 we typically used H_2 at ~4000 psi (280 atm) for two days while heating the fiber to 70–80 °C. This temperature was not high enough to initiate thermal reduction of Ge in glass,[12] and therefore the hydrogen was incorporated into the glass in the form of H_2 molecules.

For H_2-loaded fibers, in which the photoinduced index change is large, we measured Δn by illuminating the fiber with a uniform UV light beam and measuring the shift (a few nanometers) in resonance wavelength of a weak Bragg grating previously written in the fiber. However, in fibers without H_2 the photoinduced index change is too small to measure with this method, so we used a Mach–Zehnder fiber interferometer.[13]

Figure 1 shows the spectrum of the photosensitive response of a H_2-free fiber. The refractive index increases sublinearly with UV fluence in these fibers,[14]

0146-9592/99/110729-03$15.00/0

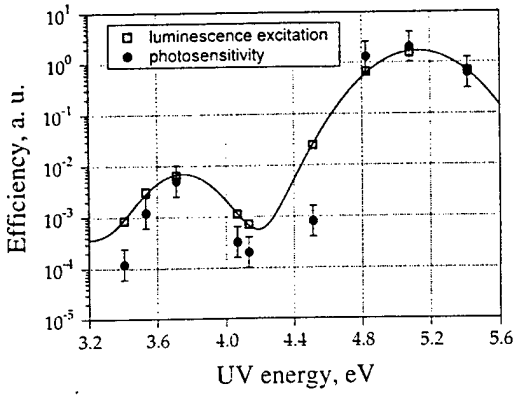

Fig. 1. Photosensitivity of H_2-free Ge-doped fiber (10% mol.) follows the excitation spectrum of the triplet state of germanium oxygen-deficient centers. The solid curve is a fit using the sum of two Gaussians.

so we define the photosensitivity as the reciprocal of the fluence required for a fixed index change of $\Delta n = 10^{-4}$. The photosensitivity has two maxima, at 3.7 and 5.1 eV, corresponding to the known absorption peaks of germanium oxygen-deficient centers. Between the two peaks at 4.2 eV the photosensitivity reaches a minimum. Also shown in Fig. 1 is the measured excitation spectrum of luminescence at 400 nm from the triplet state of the GODC. The similarity between the two curves is another confirmation that, in H_2-free fibers, the key to the photoinduced index change is the excitation of the GODC to its triplet state.

In H_2-loaded fibers the picture looks completely different; Fig. 2 shows that the photosensitivity increases almost exponentially with UV photon energy. (Here the photosensitivity is defined as the reciprocal of the fluence required for a fixed index change of $\Delta n = 3 \times 10^{-4}$.) Note the absence of the characteristic minimum at 4.2 eV that is observed in H_2-free fibers. We measured the spectral dependence of the photosensitivity at $T = 95$ K, $T = 295$ K, and $T = 375$ K and found that increasing the temperature merely shifted the spectrum and increased the photosensitivity, in accordance with what was reported in Ref. 7. The photosensitive response appears to start saturating at 5.4 eV, although the error bar on this data point was higher. Nevertheless, comparing the photosensitivity at 5.0 eV (248 nm) and 6.4 eV (193 nm) (Ref. 5) shows that the response at 6.4 eV is only ~10 times higher, which confirms the possible saturation of the photosensitivity at 6–7 eV.

In many amorphous materials the tail of the fundamental absorption, α, depends exponentially on light energy E and temperature T[15]:

$$\alpha \sim \exp(AE + T/T_1), \tag{1}$$

where A is a slope parameter and T_1 is a characteristic temperature. In particular, Trukhin and Kulis[15] found values of $A = 5.7$ eV^{-1} and $T_1 = 231$ K for defect-free pure GeO_2 glass and $A = 5.5$–8.7 eV^{-1}, $T_1 = 105$–213 K for various germanate glasses. Fitting the data in Fig. 2 to relation (1) yields $A = 6.4$ eV^{-1} and $T_1 = 133$ K, in excellent agreement with the findings reported in Ref. 15. This result indicates that it is regular Ge—O bonds and not Ge defects that determine the photosensitivity of H_2-loaded glass.

We also measured the first overtone of the OH absorption at ~1.4 μm in the UV-irradiated fibers and found that the induced OH absorption was linearly proportional to the index change (Fig. 3). The slope coefficient was ~0.6 dB/cm for $\Delta n = 10^{-3}$, independently of the Ge concentration in the core (3–20 mol. % Ge). Clearly, OH is being produced in the reaction that causes the refractive-index change, at least at $\Delta n > 10^{-4}$. In the initial stages of the reaction, when $\Delta n < 10^{-4}$, H_2 can react with GODC to produce H(II) centers (H—•Ge═).[16]

Using the known extinction coefficient for OH in silica glass [~80 L/(mol cm)],[17] we can estimate the concentration of light-induced OH. In fibers loaded with 3-mol. % H_2, the index change saturated at $\sim 1.4 \times 10^{-2}$ and ~9 mol. % OH in the core. (Although 6-mol. % OH would seem to be the maximum that is possible here, H_2 in the cladding acted as a reservoir and diffused into the core during writing). This means that one atom or possibly both atoms of each H_2 molecule were converted into OH upon UV irradiation of the glass.

There are only a few conditions in which a Ge—O bond is broken and at least one hydrogen atom is

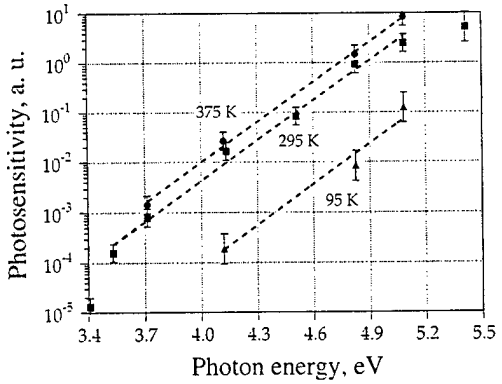

Fig. 2. Photosensitivity of H_2-loaded Ge fiber (10% mol.) increases exponentially with energy and temperature.

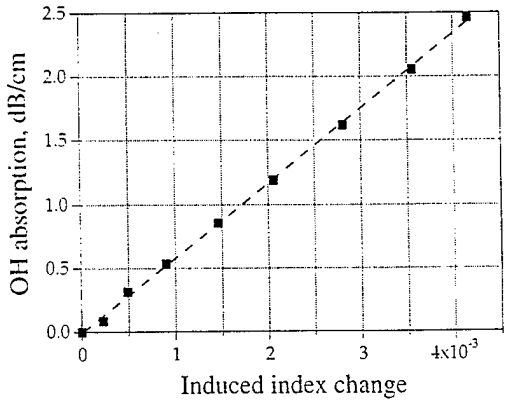

Fig. 3. Correlation of induced OH absorption with induced index change in Ge fiber (10% mol.) caused by irradiation with 300-nm light.

used to form OH. One pathway creates one OH per H_2 molecule and also produces a Ge—H bond:

$$\equiv Ge—O—Si\equiv + H—H \rightarrow \equiv Ge—H + H—O—Si\equiv. \quad (2)$$

If this were the dominant pathway, Ge—H bonds would be as abundant as OH bonds. However, Cordier *et al.*[18] recently found that the concentration of Ge—H is an order of magnitude smaller than that of OH and molecular water and that it differed from sample to sample.

An alternative pathway produces two OH groups per H_2 molecule by reducing Ge to a divalent state[12]:

$$\equiv Si—O—Ge—O—Si\equiv + H—H \rightarrow =Ge: + 2(H—O—Si\equiv). \quad (3)$$

This reaction is easily activated by heat and is widely used to increase the concentration of the GODC (=Ge:) in fibers.[4] If this were the pathway of the photoinduced reaction, we would expect a huge increase in GODC's after UV exposure. However, exactly the opposite is observed: The GODC absorption band is quickly erased by UV irradiation.[3,4] One can argue that perhaps GODC's are created but then are immediately destroyed by UV light. However, we did not observe any increase in GODC concentration even with 4.2-eV (300-nm) light, which the GODC's do not absorb (see Fig. 1).

We think that the most probable pathway involves two stages:

$$\equiv Ge—O—Si\equiv + h\nu \rightarrow \equiv Ge - \cdots - O—Si\equiv, \quad (4a)$$

$$\equiv Ge - \cdots - O—Si\equiv + H—H \rightarrow \equiv Ge\bullet + H—O—Si\equiv + H\bullet. \quad (4b)$$

First, a UV photon excites a regular Ge—O bond [reaction (4a)]. While it is excited the bond is attacked by a nearby H_2 molecule. At room temperature H_2 is known to react actively with nonbridging oxygen to form an OH group. Although nonbridging oxygen is a completely ruptured bond, it is not unreasonable to assume that H_2 can react with an excited Ge—O bond. This reaction produces Si—OH, a GeE′ center, and atomic hydrogen [reaction (4b)], as first proposed by Williams *et al.*[19] This result is in agreement with the observation of Tsai *et al.*[6] of efficient generation of GeE′ centers with UV irradiation of H_2-loaded fibers. Using the known concentration of the induced OH groups and the absorption of GeO_2 glass,[15] we estimate the quantum yield of this photoactivated reaction to be of the order of 10^{-2}. Although a fraction of the atomic hydrogen might further react with the GeE′ center to form a Ge—H bond, most of the atomic hydrogen probably participates in breaking another Ge—O bond.

In conclusion, we have investigated the photoinduced reaction of H_2 with Ge-doped glass over a wide range of UV energies and temperatures. By measuring the spectral response of glass with and without H_2, we clearly show that different microscopic mechanisms operate in these two cases. In H_2-free fibers, the index change is initiated by excitation of GODC's to their triplet state. In H_2-loaded fibers the reaction is initiated by the absorption of UV light in the tail of the fundamental band of Ge-doped glass. The excited Ge—O bond then reacts with H_2 to produce OH groups and GeE′ centers.

We acknowledge support from the U.S. Air Force Office of Scientific Research and the Joint Services Electronics Program. J. Feinberg's e-mail address is feinberg@physics.usc.edu.

References

1. G. Meltz, W. W. Morey, and W. H. Glenn, Opt. Lett. **14,** 823 (1989).
2. E. M. Dianov, D. S. Starodubov, S. A. Vasiliev, A. A. Frolov, and O. I. Medvedkov, Opt. Lett. **22,** 221 (1997).
3. P. J. Lemaire, R. M. Atkins, V. Mizrahi, and W. A. Reed, Electron. Lett. **29,** 1191 (1993).
4. R. M. Atkins, P. J. Lemaire, T. Erdogan, and V. Mizrahi, Electron. Lett. **29,** 1234 (1993).
5. J. Albert, B. Malo, F. Bilodeau, D. C. Johnson, K. O. Hill, Y. Hibino, and M. Kawachi, Opt. Lett. **19,** 387 (1994).
6. T.-E. Tsai, G. M. Williams, and E. J. Friebele, Opt. Lett. **22,** 224 (1997).
7. P. J. Lemaire, A. M. Vengsarkar, W. A. Reed, and D. J. DiGiovanni, Appl. Phys. Lett. **66,** 2034 (1995).
8. J. Martin and F. Ouelette, Electron. Lett. **30,** 811 (1994).
9. R. M. Atkins and R. P. Espindola, Appl. Phys. Lett. **70,** 1068 (1997).
10. D. S. Starodubov, V. Grubsky, J. Feinberg, and T. Erdogan, in *Conference on Lasers and Electro-Optics*, Vol. 11 of OSA Technical Digest Series (Optical Society of America, Washington, D.C., 1997), postdeadline paper CPD24.
11. V. Grubsky, D. S. Starodubov, and J. Feinberg, in *Bragg Gratings, Photosensitivity, and Poling in Glass Fibers and Waveguides: Applications and Fundamentals*, Vol. 17 of 1997 OSA Technical Digest Series (Optical Society of America, Washington, D.C., 1997), p. 98.
12. K. Awazu, H. Kawazoe, and M. Yamahe, J. Appl. Phys. **68,** 2713 (1990).
13. E. M. Dianov, S. A. Vasiliev, A. S. Kurkov, O. I. Medvedkov, and V. N. Protopopov, in *22nd European Conference on Lasers and Electro-Optics (ECOC '96)* (Institute of Electrical and Electronics Engineers, New York, 1996), p. 65.
14. V. Grubsky, A. Skorucak, D. S. Starodubov, and J. Feinberg, IEEE Photon. Technol. Lett. **11,** 87 (1999).
15. A. N. Trukhin and P. Kulis, J. Non-Cryst. Solids **188,** 125 (1995).
16. L. Skuja, J. Non-Cryst. Solids **149,** 77 (1992).
17. G. Stephenson and K. H. Jack, Trans. Br. Ceram. Soc. **59,** 397 (1960).
18. P. Cordier, C. Dalle, C. Depecker, P. Bernage, M. Douay, P. Niay, J.-F. Bayon, and L. Dong, J. Non-Cryst. Solids **224,** 277 (1998).
19. D. L. Williams, B. J. Ainslie, R. Kashyap, G. D. Maxwell, J. R. Armitage, R. J. Campbell, and R. Wyatt, Proc. SPIE **2044,** 55 (1993).

Dynamic Dispersion Compensation in a 10-Gb/s Optical System Using a Novel Voltage Tuned Nonlinearly Chirped Fiber Bragg Grating

K.-M. Feng, *Student Member, IEEE,* J.-X. Cai, *Student Member, IEEE,* V. Grubsky, D. S. Starodubov, M. I. Hayee, S. Lee, *Student Member, IEEE,* X. Jiang, *Member, IEEE,* A. E. Willner, *Senior Member, IEEE,* and J. Feinberg

Abstract—**We experimentally demonstrate dynamic dispersion compensation using a novel nonlinearly chirped fiber Bragg grating in a 10-Gb/s system. A single piezoelectric transducer continuously tunes the induced dispersion from 300 to 1000 ps/nm. The system achieves a bit-error rate = 10^{-9} after both 50 and 104 km of single-mode fiber by dynamically tuning the dispersion of the grating between 500 and 1000 ps/nm, respectively. The power penalty after 104 km is reduced from 3.5 to <1 dB.**

Index Terms—**Dispersion compensation, optical fiber communication, optical fiber dispersion, optical gratings.**

TWO OF THE MOST troublesome issues in ≥10-Gb/s optical fiber transmission are the accumulation of dispersion and nonlinearities. Dispersion-managed single-channel or wavelength-division-multiplexing (WDM) systems have been demonstrated in which the dispersion accumulated in one span of fiber is negated by an optical element that provides the opposite dispersion. The nonlinearities are controlled by always maintaining some dispersion at any given point along the fiber span. The accumulation of dispersion in high-speed optical transmission systems can be compensated either with dispersion compensating fiber (DCF) [1] or a linearly chirped fiber Bragg grating (FBG) [2]. However, the accumulated dispersion for a data channel may vary in time for: 1) dynamically reconfigurable optical networks in which a given channel may originate locally or far away, and 2) transmission systems having changing operating conditions (i.e., laser or modulator chirp). For such dynamic systems, dispersion compensation must be adjustable in order to dynamically track the accumulated dispersion. For the DCF, there is no method at present for tuning *in situ* its dispersion. For the linearly chirped FBG, simply stretching the grating only produces a shift in the resonant wavelength range of the reflected band but does nothing to change the induced dispersion. A recent report used 21 separate stretching segments to asymmetrically stretch a uniform FBG to change the induced dispersion [3].

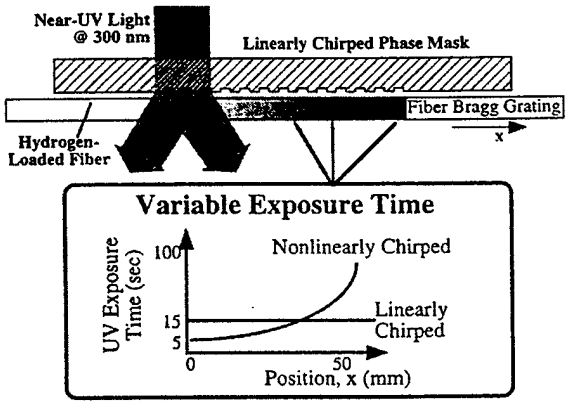

Fig. 1. Schematic for fabricating the nonlinearly chirped FBG using a linearly chirped phase mask. The exposure time is continuously varied to induce a nonlinear chirp, as shown on the inset.

In this letter, we report: 1) the fabrication and tuning characteristics of a novel *nonlinearly chirped* fiber Bragg grating in which a *single* piezoelectric transducer is used to tune the dispersion and 2) the first system demonstration of dynamic dispersion compensation for a 10-Gb/s optical channel. The time delay induced by this nonlinearly chirped FBG changes with wavelength in a nonlinear fashion. We tune the resonant wavelength of the FBG and change the generated dispersion continuously from 300 to 1000 ps/nm for a given channel. In our system demonstration, a phase modulation to amplitude modulation (PM-to-AM) technique [4] is used to dynamically determine the relative accumulated dispersion in a channel. This PM-to-AM signal drives the piezoelectric transducer to induce the appropriate amount of inverse dispersion necessary for compensation. By switching between two different lengths of single-mode fiber (SMF), the power penalty is reduced to <1 dB both for a link containing high dispersion (104 km, initial penalty = 3.5 dB) and for one containing low dispersion (50 km, initial penalty = 1.5 dB). Compensation is achieved in less than 2 ms, which is appropriate for circuit-switched networks.

Manuscript received August 17, 1998; revised November 3, 1998. This work was supported by the National Science Foundation Presidential Faculty Fellows Award, by the Packard Foundation Fellowship in Science and Engineering, by the Charles Less Powell Foundation, and by the NSF ERC in Integrated Media Systems.

K.-M. Feng, J.-X. Cai, M. I. Hayee, S. Lee, X. Jiang, and A. E. Willner are with the Department of Electrical Engineering—Systems, University of Southern California, Los Angeles, CA 90089-2565 USA.

V. Grubsky D. S. Starodubov, and J. Feinberg are with the Department of Physics and Astronomy, University of Southern California, Los Angeles, CA 90089-0484 USA. They are also with D-STAR Technologies, Inc., Manhattan Beach, CA 90266 USA.

Publisher Item Identifier S 1041-1135(99)01868-6.

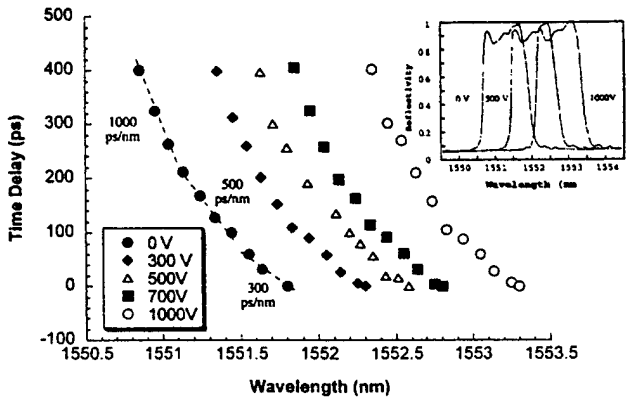

Fig. 2. Curves of time delay versus wavelength for different applied voltages of the piezoelectric stretcher. Inset: Reflected spectra for different stretching voltages.

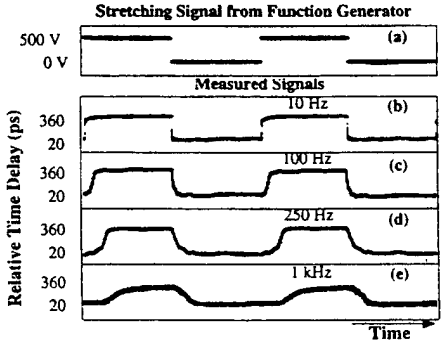

Fig. 3. Response of the dispersion compensator to an applied square-wave voltage (0–500 V) at different stretching frequencies.

The nonlinearly chirped grating is made with near-ultraviolet light at 300 nm [5]. The absorption of 300-nm light in the fiber core is sufficiently small so as to avoid damage to the core-cladding interface [6]. The photosensitive fibers are first soaked in a hydrogen chamber at 250 atm. pressure at ~60 °C for two days to give the core an estimated molecular hydrogen concentration of 2.5 mol.%. Light from an ultraviolet argon laser operating on a group of spectral lines near 300 nm is focused through a 50-mm linearly chirped phase mask onto the fiber core at ~200 W/cm^2. In order to make a nonlinearly chirped fiber Bragg grating through a linearly chirped phase mask, the distribution of the index of refraction along the grating must be nonuniform and can be locally altered by customizing the exposure time. For our nonlinearly chirped grating, each 1-mm spot along the fiber is exposed to the ultraviolet light for a variable time period ranging from 5 to 100 s (see Fig. 1). The resulting nonlinearly chirped grating is then mounted on a single piezoelectric transducer (PZT). An optical circulator diverts the grating's reflected signal for subsequent measurement. Stretching the FBG with the piezoelectric transducer tunes the effective induced dispersion.

Fig. 2 shows a family of fiber Bragg grating-induced time delay versus wavelength curves for different applied voltages to the piezoelectric transducer. For any given applied voltage, the dispersion (i.e., the *slope* of the curve at that wavelength) varies nonlinearly from 300 to 1000 ps/nm. A larger dispersion

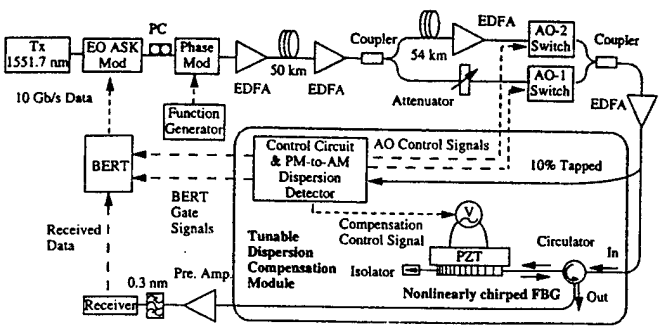

Fig. 4. Experimental setup to demonstrate dynamic dispersion compensation in a 10-Gb/s system.

range can be achieved if using a longer phase mask. Changing the applied voltage merely shifts the curve without altering its shape. For a given fixed channel wavelength, the dispersion varies with applied voltage from 300 to 1000 ps/nm. With ~1000 V applied, the reflected band is shifted by ~1.5 nm and the wavelength shift with voltage is linear. The observed grating ripple is less than ±50 ps for all time delay measurements. In our system experiment, the operating wavelength is set at 1551.7 nm. The inset in Fig. 2 is the reflected spectra under different stretching voltages. The bandwidth is ~1 nm and the reflectivity varies by ~0.7 dB.

The tuning speed of the variable dispersion compensator is measured using a 1-GHz sinusoidal input optical wave. A square-wave voltage is applied to the piezoelectric transducer in order to reflect the optical signal at two different positions along the grating, thus varying the time delay. The reflected signal is mixed with a reference signal, and the induced phase differential is monitored by an oscilloscope. Fig. 3(a) shows the scope trace of the applied voltage alternating between 0 and 500 V (corresponding to 20- and 360-ps time delay, respectively). Fig. 3(b)–(e) shows the output scope traces of the mixer using different frequencies for the applied piezoelectric transducer voltage. The compensator can follow the applied voltage up to about 250 Hz, limited by the mechanical stretching element. Therefore, dynamic compensation is achieved in less than 2 ms, making this technique suitable for highly robust dynamic systems and circuit-switched networks.

Fig. 4 shows the dynamic dispersion compensation system. The operating wavelength is set at 1551.7 nm. The signal is modulated at 10 Gb/s and passes through either 50 or 104 km of conventional singlemode fiber by alternating between two parallel paths as controlled by two acoustooptic switches (AO). A key feature of the dynamic operation is the tapping off of a small portion of the incoming signal and automatically detecting the amount of dispersion that has been accumulated and must be compensated. This is performed by using a PM-to-AM technique that introduces a 1-kHz phase modulation onto the data signal at the transmitter. After passing through a dispersive fiber, this PM signal is converted to amplitude modulation proportional to the fiber length [4]. The amplitude modulation provides a control signal for determining the amount of stretching required for the dynamic dispersion compensator. The dynamic compensation module consists of the tunable, nonlinearly chirped grating dispersion compensator, a

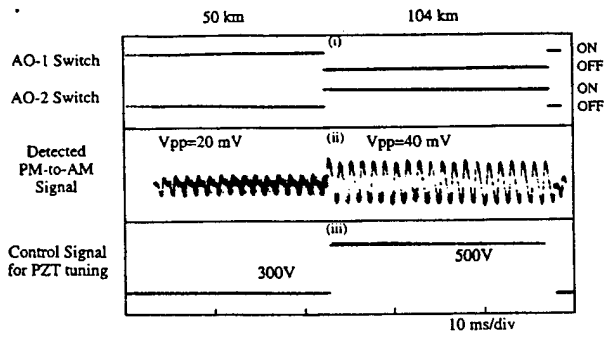

Fig. 5. Detected phase modulation to amplitude modulation (PM-to-AM) waveforms after switching between link lengths of 50 and 104 km. The corresponding piezoelectric transducer stretching voltages are also shown.

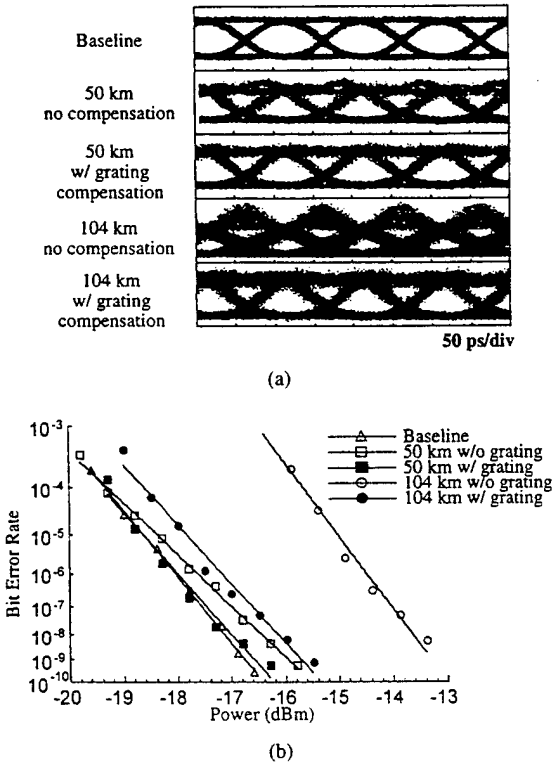

Fig. 6. (a) Eye diagrams after 0, 50, and 104 km with and without the nonlinearly chirped FBG. (b) BER measurements after 0, 50, and 104 km with and without the nonlinearly chirped FBG.

PM-to-AM dispersion detector, and a dynamic control circuit. The 1-kHz AM signal is detected by the PM-to-AM dispersion detector, which drives the dynamic control electronics and generates the appropriate piezoelectric transducer voltage for dispersion compensation.

The dispersion value for the 1551.7-nm channel is 300, 500, and 1000 ps/nm for piezoelectric transducer voltages of 0, 300, and 500 V, respectively. Fig. 5(i) shows the control signals to the two AO switches at 20-Hz modulation rate (25-ms compensation time). When AO1 is "on," the channel is transmitted through 50 km, and when AO2 is "on," the signal is transmitted through 104 km. Fig. 5(ii) is the detected PM-to-AM signal after both 50 and 104 km for which the AM signal is double for twice the length. Fig. 5(iii) is the control voltage applied to the piezoelectric transducer. The optimal tuning voltages are 300 V for 50 km and 500 V for 104 km.

By switching between 50 and 104 km of transmission fiber, we demonstrate dynamic dispersion compensation in a 10-Gb/s system. We intentionally pre-chirp the signal to optimize the BER after 50 km with nearly 0 dB power penalty at 300 V stretching voltage. Fig. 6(a) and (b) shows the eye diagrams and bit-error-rate (BER) curves under switching conditions for baseline and with and without compensation after both 50 and 104 km. Without compensation, the eye is fairly open after 50 km, whereas the eye is closing after 104 km. After tunable compensation, the eyes are all open. The BER $= 10^{-9}$ power penalty is reduced from 3.5 dB to less than 1 dB after 104 km. This 1-dB power penalty is mainly due to the nonfully compensation of the dispersion. However, only a small amount of compensation is needed for a channel passing through 50 km since less dispersion has been accumulated.

ACKNOWLEDGMENT

The authors wish to acknowledge Dr. de Silva at Corning and Dr. Frigo at AT&T for donating single-mode fiber.

REFERENCES

[1] R. J. Nuyts, Y. K. Park, and P. Gallion, "Performance improvement of 10 Gb/s standard fiber transmission system by using the SPM effect in the dispersion compensating fiber," *IEEE Photon. Technol. Lett.*, vol. 10, pp. 1406–1408, 1996.

[2] M. J. Cole, H. Geiger, R. I. Laming, S. Y. Set, M. N. Zervas, W. H. Loh, and V. Gusmeroli, "Broadband dispersion-compensating chirped fiber Bragg gratings in 10 Gbit/s NRZ 110 km nondispersion-shifted fiber link operating at 1.55 μm," *Electron. Lett.*, vol. 33, pp. 70–71, 1997.

[3] M. M. Ohn, A. T. Alavie, R. Maaskant, M. G. Xu, F. Bilodeau, and K. O. Hill, "Tunable fiber grating dispersion using a piezoelectric stack," *Conf. Optical Fiber Communication*, Dallas, TX, Feb. 1997. Washington, DC: Opt. Soc. Amer., 1997, paper WJ3.

[4] M. Tomizawa, Y. Yamabayashi, Y. Sato, and T. Kataoka, "Nonlinear influence on PM-AM conversion measurement of group velocity dispersion in optical fibers," *Electron. Lett.*, vol. 30, pp. 1434–1435, 1994.

[5] D. S. Starodubov, V. Grubsky, J. Feinberg, B. Kobrin, and S. Juma, "Bragg grating fabrication in germanosilicate fibers by use of near-UV light: A new pathway for refractive-index changes," *Opt. Lett.*, vol. 22, pp. 1086–1088, 1997.

[6] J.-L. Archambault, L. Reekie, and P. St. J. Russell, "100% reflectivity Bragg reflectors produced in optical fibers by single excimer laser pulses," *Electron. Lett.*, vol. 29, pp. 453–454, 1993.

Fabrication of Long-Period Fiber Gratings with No Harmonics

V. Grubsky, A. Skorucak, D. S. Starodubov, and J. Feinberg

Abstract— **We demonstrate a method to fabricate spectrally clean long-period gratings in optical fibers. Because the photosensitivity of glass is nonlinear, even a sinusoidal light pattern will generate harmonic gratings, and these higher order gratings can cause unwanted resonances. We solve this problem by first measuring the photosensitivity of the glass and then scanning the fiber across an ultraviolet light beam at a variable speed under computer control. The resulting spectra are free from extraneous resonances caused by harmonics of the fundamental grating period.**

Index Terms—**Fiber gratings, index of refraction, optical fiber filters, optical fibers.**

LONG-PERIOD fiber gratings [1], [2] can couple light between copropagating modes of an optical fiber and are used as nonreflecting band-rejection filters [1], bandpass filters [3], optical sensors [4], and gain flatteners for erbium-doped amplifiers [5]. For most applications, the quality of the grating spectrum is crucial. Nevertheless, the transmission spectrum of a long-period grating is often contaminated by extraneous resonances. These extra resonances can lie in the midst of the spectral region of interest and so can mar the spectrum like graffiti mars a painting. In this letter, we show that some of these extra resonances are caused by unwanted harmonics of the fundamental grating period. We also show that because glass has a nonlinear response to light, simple sinusoidal illumination of the glass fiber will not eliminate these harmonics. Finally we demonstrate a method to eliminate these unwanted resonances using a specially designed exposure system.

Here, we consider a long-period grating with period Λ chosen to match the difference in effective refractive indices of the single-mode core and a copropagating cladding mode. A common way of imprinting a long-period grating into an optical fiber is to expose the fiber core to ultraviolet (UV) light from the side through an amplitude mask of spatial period Λ. Variations include using photolithographic chrome-on-silica masks [1], etched dielectric mirrors [6], or microcontact printing of the masks onto the fiber surface [7]. An alternative method to fabricate fiber gratings is to write the desired index pattern point by point by translating the fiber relative to a focused UV light beam [8], [9] and periodically turning the laser beam on and off. In all of these cases, the grating is a square wave, and so it contains an unhealthy dose of odd harmonics. Such square-wave long-period gratings will couple modes not only at the desired wavelength but also at additional wavelengths determined by higher harmonics of the fundamental grating period.

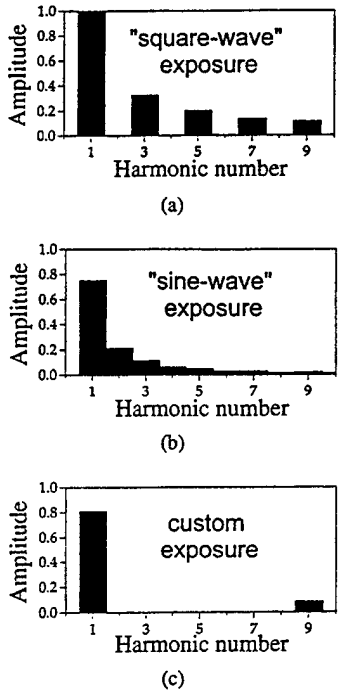

Fig. 1. Harmonic content of index change resulting from various light patterns: (a) square-wave; (b) sine-wave; and (c) custom exposure schedule. The coefficients are normalized by the amplitude of the first harmonic of the square-wave grating. Note that even the sine-wave light pattern produces appreciable harmonic amplitudes, while the harmonic components are virtually eliminated in the custom exposed fiber. [The custom exposure used ten steps to approximate the desired pattern, causing the ninth harmonic seen in (c).]

The response of germanosilicate glass to UV irradiation is highly nonlinear. Typically, the photoinduced change of refractive index Δn caused by exposure to a fluence F obeys a power law [10]

$$\Delta n = AF^B. \tag{1}$$

The coefficients A and B in (1) depend on the composition of the fiber and the UV wavelength used for irradiation. This nonlinear photosensitivity of glass fibers makes fabrication of a harmonic-free, long-period grating nontrivial, *because even a sinusoidal light pattern will produce a nonsinusoidal index pattern.* Fig. 1(a) and (b) show the amplitude of the harmonic

Manuscript received July 22, 1998; revised September 18, 1998.

V. Grubsky, A. Skorucak, and J. Feinberg are with D-STAR Technologies, Inc., Manhattan Beach, CA 90266 USA, and also with the Department of Physics, University of Southern California, Los Angeles, CA 90089-0484 USA.

D. S. Starodubov is with D-STAR Technologies, Inc., Manhattan Beach, CA 90266 USA.

Publisher Item Identifier S 1041-1135(99)00376-6.

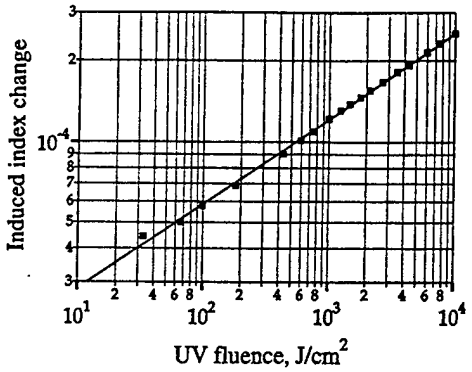

Fig. 2. Light-induced index change versus CW fluence in a 10% Ge-doped fiber using 244–nm UV light. This log–log plot confirms a power-law dependence with a slope of 0.32.

gratings created with square-wave and with sinusoidal illumination. Although the harmonics are reduced in the sinusoidal pattern they are still prominent. In order to make a purely sinusoidal index pattern Δn in the fiber, we must compensate the known nonlinear photosensitivity of the fiber with a custom UV exposure schedule.

We first measure a fiber's nonlinear photosensitivity using a Mach–Zehnder interferometric technique [11]. Fig. 2 shows that for 244-nm light and with no hydrogen loading we obtain a fit to (1) with $A = 1.37 \times 10^{-5}$ and $B = 0.32$, independent of the intensity of the writing light. (The ~10% Ge-doped fiber with NA ~ 0.2 was obtained from the Fiber Optic Research Center, Moscow, Russia.) For 344-nm light, we obtain $A = 1.97 \times 10^{-5}$ and $B = 0.27$ (using PFBG-1355-T fiber with NA = 0.3, core diameter = 2.3 μm from QPS Technology, Canada). In general, $B \sim 0.25 - 0.35$, so the index always grows nonlinearly with fluence in fibers without hydrogen.

To create a purely sinusoidal index pattern in the fiber we compensate the known nonlinear response of the fiber with a custom UV exposure schedule. We divide each grating period into discrete sections. (We used 10.) In each section, we scan the fiber at a constant speed past a focused UV beam using a computer-controlled motorized translation stage. Using photosensitivity data (such as shown in Fig. 2) the computer calculates the optimum scanning speed for each section to produce refractive-index steps that approximate the desired sinusoidal index variation. Fig. 1(c) shows the harmonic amplitudes of Δn using this custom profile. Note that the harmonic grating amplitudes are now essentially eliminated.

Fig. 3(a) shows the spectrum obtained with a simple square-wave grating; it has an extraneous resonance smack in the middle of the spectrum. This particular resonance is due to the third harmonic of the fundamental grating coupling to the $HE_{1,14}$ cladding mode (as determined by our numerical simulation of the cladding mode resonances in this fiber). Fig. 3(b) demonstrates the impressively clean transmission spectrum obtained using the computer-generated long-period grating. Note that the extraneous resonance has been eliminated. (The weaker satellite resonances seen on the long wavelength side of each peak are caused not by our grating fabrication technique but by minute imperfections of this fiber.)

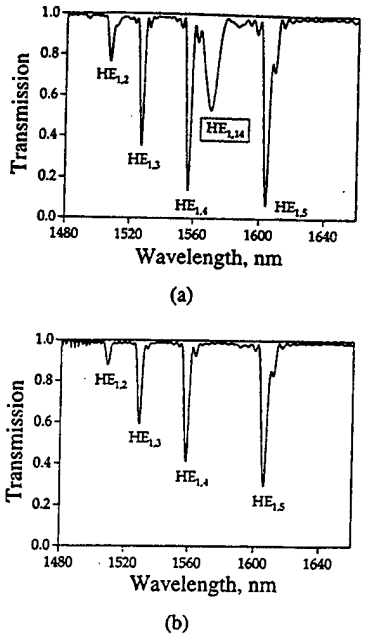

Fig. 3. Measured transmission spectra (Ando AQ-6315B spectrum analyzer, 0.5-nm resolution) of a long-period grating written in QPS fiber with a (a) square-wave index pattern and (b) computer-generated index pattern. The extraneous resonance lying smack in the middle of the spectrum of (a) is caused by the third-harmonic grating coupling to the $HE_{1,14}$ cladding mode, and it is eliminated in (b). Grating period = 305 μm; grating length = 3.4 cm; laser power = 200 mW; λ = 334 nm.

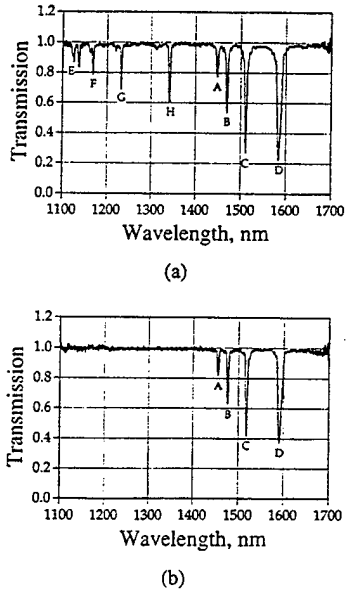

Fig. 4. Measured transmission spectra (2 nm resolution) of a long-period grating written in fiber from Fiber Optic Research Center, Moscow, Russia with (a) a square-wave index pattern and (b) a computer-generated index pattern. Here, the extraneous resonances labeled E–H all spring up at shorter wavelengths; they are caused by the third-harmonic grating. Note that the extraneous resonances are suppressed in (b). Grating period = 540 μm; grating length = 5 cm; laser power = 5.5 mW; λ = 244 nm.

Fig. 4(a) shows another example of grating harmonics. The peaks A through D are due to coupling with the fundamental grating, while the peaks E through H are due to coupling with the third-harmonic grating. Fig. 4(b) shows that the third-harmonic resonances are eliminated when the correct grating exposure schedule is used.

In conclusion, we have shown that some of the extraneous resonances seen in fibers with long-period gratings are caused by higher order harmonics of the grating's fundamental spatial frequency, and these contaminating resonances can be eliminated by careful exposure of the glass. A sinusoidal illumination schedule is not sufficient. Only by first measuring the nonlinear response of the glass fiber to UV light and then compensating the nonlinearity with a custom exposure schedule can the extraneous resonances be suppressed. This technique should prove useful for producing long-period grating filters with clean and predictable spectra.

REFERENCES

[1] A. M. Vengsarkar, P. L. Lemaire, J. B. Judkins, V. Bhatia, T. Erdogan, and J. E. Sipe, "Long-period fiber gratings as band-rejection filters," *J. Lightwave Technol.*, vol. 14, pp. 58–65, Jan. 1996.

[2] T. Erdogan, "Cladding-mode resonances in short- and long-period fiber grating filters," *J. Opt. Soc. Amer. A*, vol. 14, no. 8, pp. 1760–1773, 1997.

[3] D. S. Starodubov, V. Grubsky, A. Skorucak, J. Feinberg, K.-M. Feng, J.-X. Cai, and A. E. Wilner, "Novel fiber amplitude modulators in dynamic channel power equalization in WDM systems," in *OSA Tech. Dig. Ser., Optical Fiber Communication Conf.*, 1998, vol. 2, postdeadline paper PD8.

[4] V. Bhatia and A. M. Vengsarkar, "Optical fiber long-period sensors," *Opt. Lett.*, vol. 21, no. 9, pp. 692–694, 1996.

[5] A. M. Vengsarkar, J. R. Pedrazzani, J. B. Judkins, P. J. Lemaire, N. S. Bergano, and C. R. Davidson, "Long-period fiber-grating-based gain equalizers," *Opt. Lett.*, vol. 21, no. 5, pp. 336–338, 1996.

[6] H. J. Patrick, C. G. Askins, R. W. McElhalon, and E. J. Friebele, "Amplitude mask patterned on an excimer laser mirror for high intensity writing of long period fiber gratings," *Electron. Lett.*, vol. 33, no. 13, pp. 1167–1168, 1997.

[7] J. A. Rogers, R. J. Jackman, G. M. Whitesides, J. L. Wagener, and A. M. Vengsarkar, "Using microcontact printing to generate amplitude photomasks on the surfaces of optical fibers: A method for producing in-fiber gratings," *Appl. Phys. Lett.*, vol. 70, no. 1, pp. 7–9, 1997.

[8] K. O. Hill, B. Malo, K. A. Vineberg, F. Bilodeau, D. C. Johnson, and I. Skinner, "Efficient mode conversion in telecommunication fiber using externally written gratings," *Electron. Lett.*, vol. 26, no. 16, pp. 1270–1272, 1990.

[9] E. M. Dianov, D. S. Starodubov, S. A. Vasiliev, A. A. Frolov, and O. I. Medvedkov, "Refractive-index gratings written by near-ultraviolet radiation," *Opt. Lett.*, vol. 22, no. 4, pp. 221–223, 1997.

[10] D. Z. Anderson, V. Mizrahi, T. Erdogan, and A. E. White, "Production of in-fiber gratings using a diffractive optical element," *Electron. Lett.*, vol. 29, no. 6, pp. 566–568, 1993.

[11] E. M. Dianov, S. A. Vasiliev, A. A. Frolov, and O. I. Medvedkov, "Germanosilicate glass refractive index change under singlet and triplet excitation of germanium oxygen deficient centers," in *OSA Tech. Dig. Ser., Bragg Grating, Photosensitivity, and Poling in Glass Fibers and Waveguides: Applications and Fundamentals*, 1997, vol. 17, pp. 175–177.

MEASUREMENT OF THE TEMPORAL DELAY OF A LIGHT PULSE THROUGH A ONE-DIMENSIONAL PHOTONIC CRYSTAL

Shamino Wang,[1] Hernan Erlig,[1] Harold R. Fetterman,[1] Eli Yablonovitch,[1] Victor Grubsky,[2] Dmitry S. Starodubov,[2] and Jack Feinberg[2]
[1] Department of Electrical Engineering
University of California
Los Angeles, California 90095
[2] Department of Physics
University of Southern California
Los Angeles, California 90089-0484

Received 4 June 1998

ABSTRACT: *We measure a maximum group delay of 22.6 ps for a light pulse propagating through a 1 cm long fiber Bragg grating when the frequency of the light is tuned near the band edge of the grating. Our measurements are performed in the time domain with single picosecond resolution using wavelength-tunable pulses of 0.5 nm bandwidth spectrally sliced from a mode-locked laser. Our experimental results are qualitatively confirmed by our numerical simulations. Promising applications include optical delay elements for phased-array radar and encoders/decoders in spread-spectrum code-division multiple-access systems.* © 1999 John Wiley & Sons, Inc. Microwave Opt Technol Lett 20: 17–21, 1999.

Key words: *group delay; fiber Bragg grating; photonic crystal; wavelength slicing; code-division multiple access*

A one-dimensional photonic crystal is a periodic array of layers with different indexes of refraction. Light propagating at frequencies near the stopband of a photonic crystal will be delayed and dispersed [1], which may prove useful for optically controlled phased-array radars [2]. To date, experimental efforts to measure such delays have been in the frequency domain [3], or in the time domain with a 50 GHz sampling oscilloscope [4]. In this paper, we directly measure the group delay in the time domain with single picosecond resolution, and show that the delay increases as the frequency of the pulse approaches the edge of the photonic crystal's stopband.

We used a Bragg grating in an optical fiber as the one-dimensional photonic crystal. The grating measured ~1 cm in length, had a 1553.20 nm central wavelength, and a 2.10 nm, 3 dB bandwidth. We first theoretically analyzed the physical properties of such a structure using a commercial grating simulation program (IFO_Gratings). To match the actual grating's spectral characteristics, our simulated fiber Bragg grating had a 1 cm long uniform quarter-wave structure and a 0.0035 refractive index change between layers. Figure 1 shows the transmission spectrum and the group velocity as a function of wavelength for the simulated grating. The computed group velocity is seen to drop sharply as the central wavelength of the pulse approaches the edge of the bandgap. Therefore, a tunable delay can be achieved by varying the central wavelength of the propagating pulse with respect to the reflection edge of the grating.

To measure the delay induced by the actual grating, we used the tunable picosecond source shown in Figure 2. The 1.55 μm mode-locked erbium-doped fiber laser emitted a 160 fs (FWHM) pulse train with a 56 nm (FWHM) bandwidth. For the experiments here, we needed a tunable source whose bandwidth was smaller than the width of the grating stopband, which is usually on the order of nanometers. To narrow the frequency spectrum of our pulsed laser, we used an HP 71451B optical spectrum analyzer as a wavelength slicer [5]. By selecting the resolution bandwidth of the spectrum analyzer, we could vary the pulse bandwidth from 0.1 to 10 nm. The pulse center wavelength was tuned by selecting slices of different spectral content. An autocorrelator and a second spectrum analyzer were used to perform diagnostic tests. The results are shown in Figure 3. Note that as the pulse's spectral bandwidth decreased, its temporal length increased, as required by the uncertainty principle.

Light from the wavelength-tunable picosecond source was split into two beams. One beam was sent into the fiber containing a Bragg grating, and the other beam was sent into a reference fiber. The two transmitted signals were recombined and sent to an autocorrelator with a scan window ~120 ps. The autocorrelator displayed both the autocorrelation and the cross-correlation traces. The length of the grating arm was made intentionally longer (by ~1 cm) to separate the autocorrelation and cross-correlation traces (by ~56 ps). Any group delay caused by the fiber Bragg grating produced an additional displacement of the cross-correlation trace relative to the autocorrelation trace. The cross-correlation trace also revealed any dispersion caused by propagation through the grating. Note that any dispersion caused by the fiber itself was common to both pulses.

A typical transmission spectrum of the fiber Bragg grating is shown in Figure 4(a). The spectrum analyzer bandwidth was set to chop 0.5 nm wide wavelength slices; the resulting pulses had a ~16 ps (FWHM) autocorrelation. The chopped slices were not Gaussian, and fitted approximately the sinc-squared function predicted from a "top hat" spectral distribution over the range considered here. Correlation traces were obtained as the pulse's central wavelength was positioned at various wavelengths near the grating bandgap. For trace *A* in Figure 4(b), we expected and saw no additional delay from the grating. However, the measured group delays for points *B*, *C*, and *D* increased from the 56 ps value by 1.9, 11.4, and 22.6 ps, respectively, as the central wavelength of the pulse approached the edge of the grating's stopband.

From our simulation, we expected the following trends as the laser wavelength neared the grating bandgap: 1) increasing group velocity delay, 2) increasing dispersion, and 3) reduced transmission due to increased reflectivity nearer the grating. Indeed, traces *B*, *C*, and *D* confirm that: 1) the cross-correlation peaks moved further away from the autocorrelation traces, 2) the cross-correlation traces spread out in time due to increased dispersion, and 3) the peak intensities of the cross-correlation traces dropped because of lower transmission as the bandgap was approached. Similar trends were also observed as the bandgap was approached from

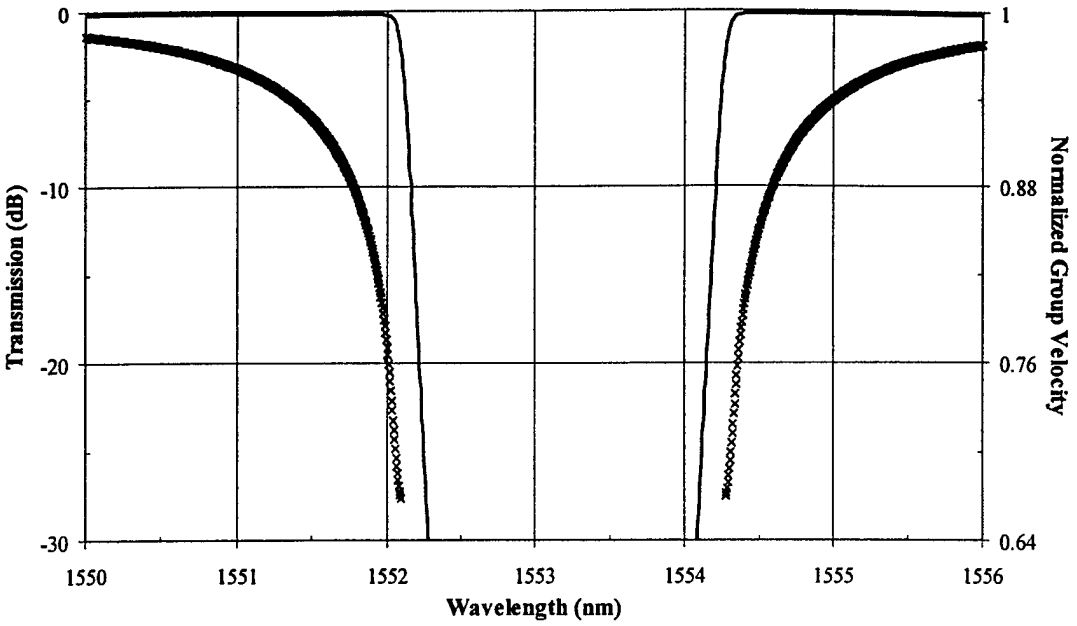

Figure 1 Simulation of a fiber Bragg grating centered at 1553.20 nm with a rectangular index profile. The solid line represents the transmission spectrum and the crosses the group velocities. A refractive index difference between layers of $\Delta n = 0.0035$ was used to match the measured spectrum. The group velocities are normalized to the speed of light in bare fiber

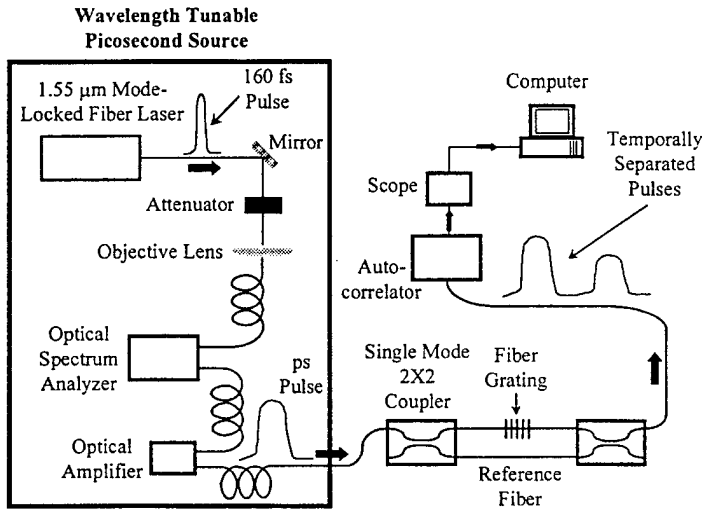

Figure 2 Group delay measurement setup. The autocorrelator displays both the autocorrelation and cross-correlation traces, with the separation between the traces equal to the temporal separation between the reference pulse and the lagging grating pulse

longer wavelengths, as shown in Figure 4(c). The measured additional group delays for points E and F were 8.2 and 3.1 ps, respectively.

Here, we have clearly demonstrated directly in the time domain that a photonic band structure can serve as a delay line in transmission. The 22.6 ps group delay caused by the grating used here corresponded to a 50% increase in the grating's effective length. That is, the 1 cm Bragg grating was equivalent to a 1.5 cm long delay line. We expect longer delays as the grating parameters are optimized in future experiments. One application for such delay lines is in phased-array radar systems, where the conventional chirped gratings and circulators/couplers might be replaced by simple uniform Bragg gratings.

It has also been proposed that photonic bandgap materials could be used as dispersion compensators [3, 6, 7]. By differentiating the group velocity with respect to wavelength, we find negative group velocity dispersion on the short-wavelength side of the grating bandgap and positive group velocity on the long-wavelength side. In principle, we can design a grating pair with different stopband locations such that positive dispersion from the first grating would compensate negative dispersion from the second grating [8]. In addition, one could put a grating in a transmitter and a second conjugate

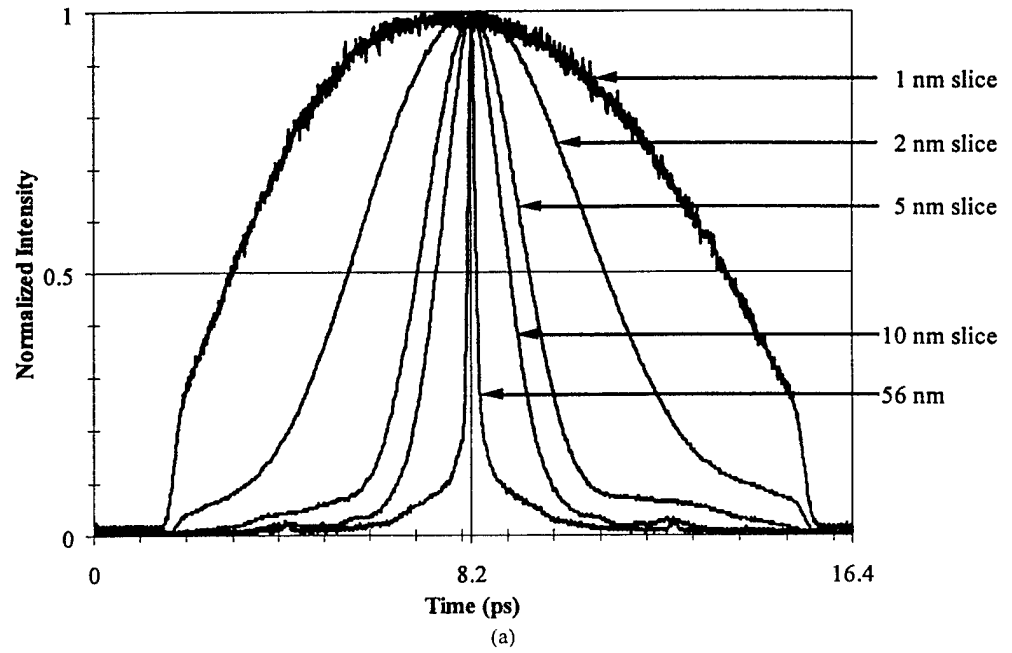

(a)

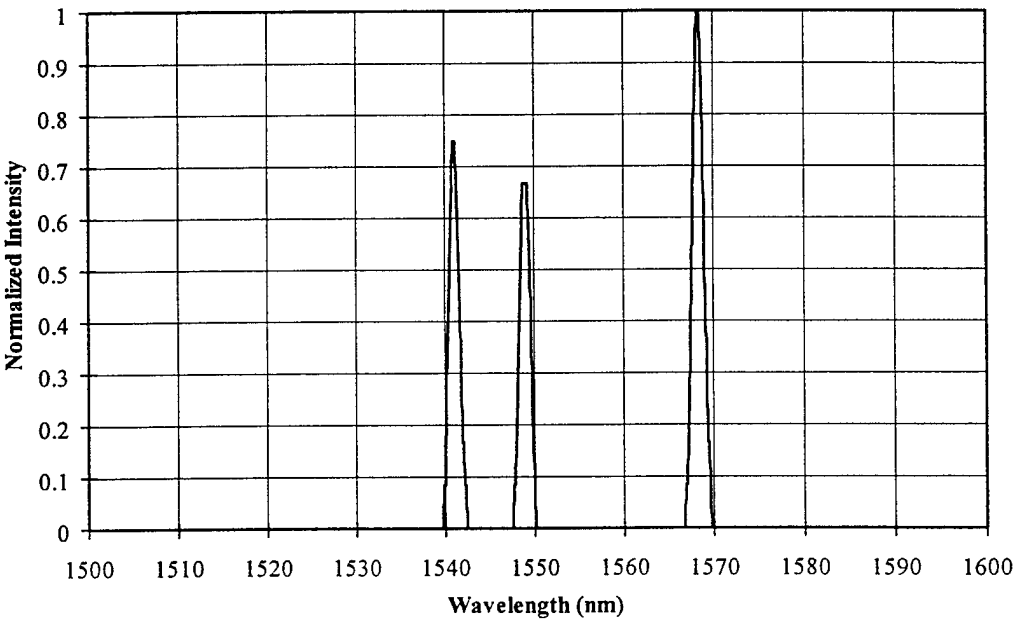

(b)

Figure 3 (a) Autocorrelation traces of the 56 nm (FWHM) bandwidth laser pulse and of various wavelength slices. (b) Tunability of a fixed bandwidth slice within the available 56 nm (FWHM) laser bandwidth

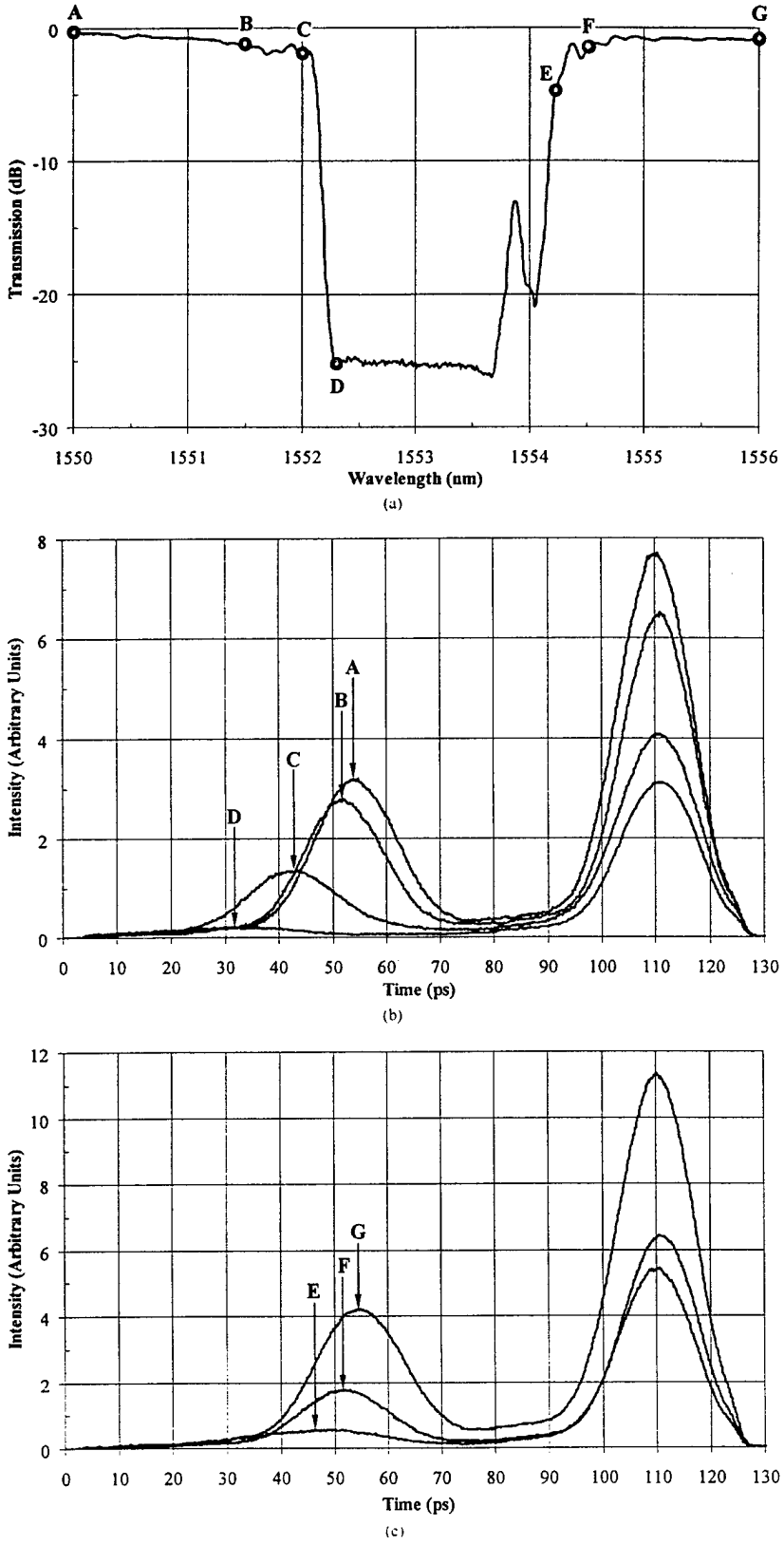

Figure 4 (a) Transmission spectrum of the fiber Bragg grating under test. Operating wavelengths for the points of interest are *A*: 1550.00 nm. *B*: 1551.50 nm. *C*: 1552.00 nm. *D*: 1552.25 nm. *E*: 1554.20 nm. *F*: 1554.50 nm, and *G*: 1556.00 nm. (b) Correlation traces for points *A*. *B*. *C*. and *D*. The autocorrelation traces are located at 110 ps. (c) Correlation traces for points *E*, *F*, and *G*. The autocorrelation traces are located at 110 ps

grating in a receiver for use as encoding/decoding components for spread-spectrum code-division multiple-access matched filter systems.

In conclusion, for the first time, to our knowledge, we have measured in the time domain, with single picosecond resolution, the group velocity delay caused by a pulse propagating near the edge of the stopband of a one-dimensional photonic crystal. Such delays can have practical applications for phased-array radar and matched filter systems.

ACKNOWLEDGMENT

This research was supported by the Air Force Office of Scientific Research (AFOSR) and by the Ballistic Missile Defense Organization (BMDO).

REFERENCES

1. M. Scalora, R.J. Flynn, S.B. Reinhardt, R.L. Fork. M.J. Bloemer, M.D. Tocci, C.M. Bowden, H.S. Ledbetter, J.M. Bendickson, J.P. Dowling, and R.P. Leavitt, Ultrashort pulse propagation at the photonic band edge: Large tunable group delay with minimal distortion and loss, Phys Rev E 54 (1996), R1078–R1081.
2. W.H. Loh, R.I. Laming, N. Robinson, A. Cavaciuiti, F. Vaninetti, C.J. Anderson, M.N. Zervas, and M.J. Cole, Dispersion compensation over distances in excess of 500 km for 10-Gb/s systems using chirped fiber gratings, IEEE Photon Technol Lett 8 (1996), 944–946.
3. B.J. Eggleton, T. Stephens, P.A. Krug, G. Dhosi, Z. Brodzeli, and F. Ouellette, Dispersion compensation using a fibre grating in transmission, Electron Lett 32 (1996), 1610–1611.
4. B.J. Eggleton, C.M. de Sterke, and R.E. Slusher, Nonlinear pulse propagation in Bragg gratings, J Opt Soc Amer B 14 (1997), 2980–2993.
5. T.M. Goyette, W. Guo, F.C. De Lucia, J.C. Swartz, H.O. Everitt, B.D. Guenther, and E.R. Brown, Femtosecond demodulation source for high-resolution submillimeter spectroscopy, Appl Phys Lett 67 (1995), 3810–3812.
6. N.M. Litchinitser, B.J. Eggleton, and D.B. Patterson, Fiber Bragg gratings for dispersion compensation in transmission: Theoretical model and design criteria for nearly ideal pulse recompression, J Lightwave Technol 15 (1997), 1303–1313.
7. N.M. Litchinitser and D.B. Patterson, Analysis of fiber Bragg gratings for dispersion compensation in reflective and transmissive geometries, J Lightwave Technol 15 (1997), 1323–1328.
8. S. Wang, H. Erlig, H.R. Feterman, E. Yablonovitch, V. Grubsky, D.S. Starodubov, and J. Feinberg, submitted to IEEE Microwave Guided Wave Lett.

CCC 0895-2477/99

Long-period fiber gratings with variable coupling for real-time sensing applications

Victor Grubsky and Jack Feinberg

Department of Physics, University of Southern California, Los Angeles, California 90089-0484, and D-STAR Technologies, Inc., 725 33rd Street, Manhattan Beach, California 90266

Received October 7, 1999

We demonstrate a long-period grating whose resonance varies in strength but remains fixed in wavelength with either temperature or strain. Using this fiber-grating sensor, we resolved a change of 1 $\mu\epsilon$ of strain or 0.04 °C in temperature. Such sensors require no spectrometer or other frequency-selective components and can operate in real time. © 2000 Optical Society of America

OCIS codes: 060.2370, 060.2400, 060.2340, 350.2770.

Long-period fiber gratings[1] can couple light between copropagating core and cladding modes of an optical fiber. Sensors using long-period fiber gratings monitor changes in temperature, strain, or refractive index, usually by measuring a shift in the grating's resonant wavelength (because the strength of the resonance usually remains constant).[2] Here we demonstrate a long-period grating sensor with just the opposite properties: its resonant wavelength remains fixed but its coupling strength varies with strain or temperature. The principal advantages of this sensor are that (1) it needs no spectrometer or other dispersive device, (2) it can be used for real-time measurements, and (3) it is sensitive.

To couple light efficiently between a core mode and a cladding mode at a resonant wavelength λ_{res} requires that the period of a long-period grating Λ satisfy a phase-matching condition:

$$\Phi(\lambda) \equiv 2\pi(n_{co} - n_{cl})/\lambda_{res} = 2\pi/\Lambda, \qquad (1)$$

where n_{co} is the effective index of the core mode and n_{cl} is the effective index of the cladding mode. Figure 1 is a plot of the intermodal dispersion function $\Phi(\lambda)$ for a typical fiber. The resonances between the core mode and a given cladding mode can be determined graphically as the intersection(s) of the intermodal dispersion function with the grating spatial frequency $2\pi/\Lambda$. For coupling between the core mode and cladding mode 1 in Fig. 1, the resonant wavelength λ_{res} is a monotonically decreasing function of grating spatial frequency. Therefore, if one alters the grating period by stretching the fiber, the resonant wavelength shifts to a new value. Most fiber strain sensors operate in this manner, and measuring the change in resonant wavelength requires using a spectrometer. However, for some combinations of core and cladding modes, Eq. (1) maps out a parabola, as shown for cladding mode 2 in Fig. 1. For operation near the base of this parabola, any change in the strain or the temperature of the grating alters the coupling strength between the core and cladding modes but leaves the resonant wavelength fixed.

The change in resonant wavelength caused by a small change in grating period can be found by a Taylor expansion of the mode dispersion function in the vicinity of λ_{res}:

$$\Phi(\lambda) - \Phi(\lambda_{res}) = a_1(\lambda - \lambda_{res}) + a_2(\lambda - \lambda_{res})^2 + \ldots. \qquad (2)$$

The first term is usually the largest, and these linear-dispersion gratings give monotonic curves like that of mode 1 in Fig. 1. All conventional long-period gratings fall into this category. The resonant wavelength changes linearly with a change in period:

$$\delta\lambda \approx -\frac{2\pi}{a_1\Lambda^2}\,\delta\Lambda. \qquad (3)$$

However, it is possible to find modes for which the linear coefficient of Eq. (2) vanishes ($a_1 = 0$) at a specific

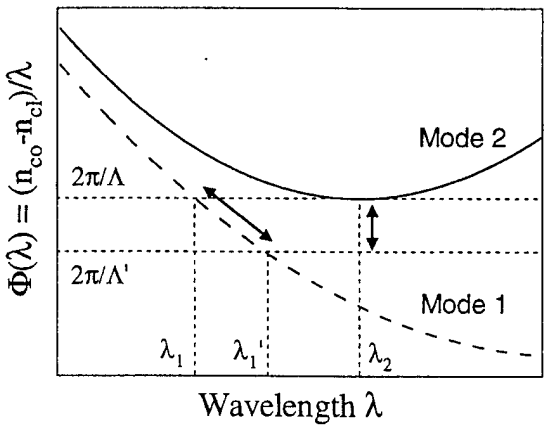

Fig. 1. Long-period grating resonances for core–cladding mode coupling are found graphically by the intersection of the intermodal dispersion function $\Phi(\lambda)$ and the horizontal line representing the spatial period of the grating. For cladding mode 1 the resonance shifts from λ_1 to λ_1' as the grating period shifts from Λ to Λ'. However, for cladding mode 2 the resonant wavelength remains fixed at λ_2 as the grating period is changed, although the strength of the resonance varies. This coupling between the core mode and cladding mode 2 has a quadratic-dispersion resonance.

0146-9592/00/040203-03$15.00/0

resonant wavelength. In this case the quadratic term a_2 dominates, and we obtain

$$\delta\lambda \approx \pm\left(-\frac{2\pi}{a_2\Lambda^2}\,\delta\Lambda\right)^{1/2}. \quad (4)$$

In Fig. 1 the curvature of the intermodal dispersion function for mode 2 is positive, so $a_2 > 0$. Therefore for $\delta\Lambda < 0$ there will be two values of $\delta\lambda$ (i.e., the resonance splits into two peaks),[3,4] but for $\delta\Lambda > 0$ there will be no resonance. The latter case is a quadratic-dispersion resonance. As the grating period increases from Λ to Λ', the resonance is lost. However, when a quadratic-dispersion grating is only a little off resonance, there can still be significant coupling between the core and the cladding modes because the limited length of the fiber grating imparts some uncertainty to the grating period. Coupling still occurs between the core and the cladding modes, although with smaller efficiency. As the grating period is changed, the amount of coupling varies but the wavelength of maximum coupling remains fixed.

Therefore we distinguish three types of long-period grating: positive linear-dispersion gratings ($d\lambda_{res}/d\Lambda > 0$), negative linear-dispersion gratings ($d\lambda_{res}/d\Lambda > 0$), and quadratic-dispersion gratings ($d\lambda_{res}/d\Lambda = 0$). In Fig. 1 the coupling between the core and cladding mode 1 always has a resonance with positive linear dispersion. The behavior of core–cladding resonance with mode 2 is more complicated: for $\lambda < \lambda_2$ it has positive linear dispersion, at $\lambda \approx \lambda_2$ it has quadratic dispersion, and for $\lambda > \lambda_2$ it has negative linear dispersion.

Why does the coupling between the core and cladding mode 2 change its character with wavelength? The intermodal dispersion function $\Phi(\lambda)$ acquires its wavelength dependence from λ in the denominator and the wavelength-dependent effective indices in the numerator [Eq. (1)]. At shorter wavelengths the core mode is concentrated primarily in the core, which makes the mode's effective index n_{co} close to that of the core, n_1. At longer wavelengths the core mode tends to spread out into the cladding, and its effective index approaches that of the cladding, n_2. Therefore the range of effective index of the core mode is $n_2 < n_{co} < n_1$. In a similar fashion the effective index of the cladding mode n_{cl} decreases with wavelength, remaining between the refractive indices of the cladding and the jacket, $n_3 < n_{cl} < n_2$. Typical values of the refractive indices in the infrared region are $n_1 \approx 1.45$, $n_2 \approx 1.44$, and $n_3 \approx 1.00$ (with the jacket removed and air surrounding the fiber). As a consequence, the effective index of the core mode n_{co} has almost no room to vary (1.44–1.45), whereas the index of the cladding mode n_{cl} can vary widely (1.00–1.44). For increasing λ, the strong decrease of the cladding mode's index (especially pronounced for high-order cladding modes) increases the numerator of intermodal dispersion function $\Phi(\lambda)$ [Eq. (1)] and eventually overcomes the growth of its denominator. This switches the sign of the slope of this function. The quadratic dispersion case occurs when these two effects exactly balance.

Our calculations suggest that, for each cladding mode of a fiber, there is a specific wavelength at which the dispersion of the core–cladding resonance switches from positive to negative. With increasing order of the cladding mode, this turning point shifts to a shorter wavelength.

Theoretically, each core–cladding resonance must have another turning point in the mid or far IR at which the dispersion switches from negative back to positive. Indeed, at long wavelengths, $n_{co} \approx n_2 = 1.4$ and $n_{cl} \approx n_3 = 1.00$, so the numerator of the dispersion function will stop increasing and λ in the denominator will take over again. Intermodal dispersion function $\Phi(\lambda)$ will begin to decrease with wavelength and eventually return to the positive-dispersion regime. However, this second turning point must be too far in the IR ($\lambda > 10\ \mu$m) to be observed; the high absorption in this region prevents propagation of light in silicate fibers.

To fabricate a quadratic-dispersion grating we used photosensitive fiber QPS-PFBG-1355-T from QPS Tech (Canada). The fiber had a N.A. of 0.3 and a core diameter $d = 2.3\ \mu$m. We exposed the fiber to 334-nm (near-UV) radiation to fabricate a grating with period $\Lambda = 50.1\ \mu$m and length $L = 1$ cm. After the grating was written, we tested its performance under strain. Figure 2 shows that the coupling efficiency of the grating changed drastically with strain, while the wavelength of the resonance remained fixed. For relatively small strain, the coupling efficiency at 1415 nm was ~80%. With increasing strain the coupling dropped, until at 9410 $\mu\epsilon$ the grating peak disappeared completely. Note that for all values of strain the best coupling was always obtained at the same fixed wavelength, 1415 nm. The slight asymmetry of the spectrum, especially pronounced for the lowest strain (1650 $\mu\epsilon$), is due to variation of the mode coupling with wavelength.

We tested the performance of a similar grating as a strain sensor. We fabricated a different quadratic-dispersion grating, using the same fiber, with period $\Lambda = 69.4\ \mu$m. This grating had a resonance

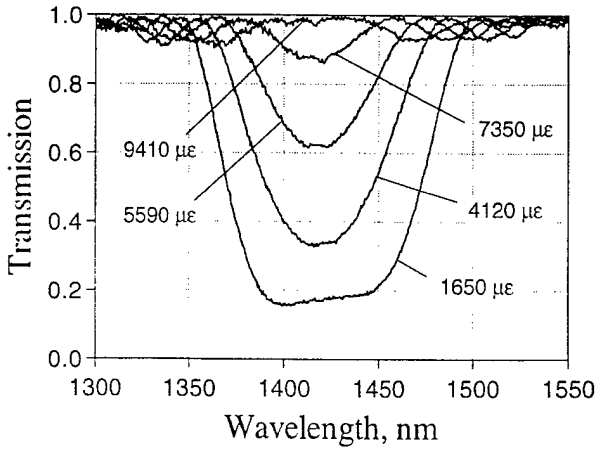

Fig. 2. Change of the transmission spectrum of a quadratic-dispersion long-period grating under strain (from 1650 to 9410 $\mu\epsilon$). The strength of the grating diminishes under increasing strain, but the resonant wavelength remains pinned at 1420 nm.

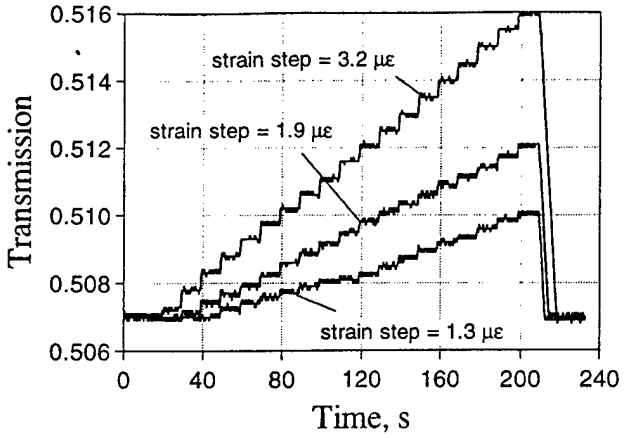

Fig. 3. Change of transmission through a quadratic-dispersion long-period grating under increasing strain. The strain is increasing linearly with time in discrete steps. The three traces have different strain steps.

at ~1570 nm. We then mounted the fiber upon a computer-controlled translation stage with resolution 0.1 μm for high-precision stretching. We increased the strain in small steps and observed that the transmission through the device at 1570 nm changed in steps according to the level of strain (Fig. 3). Even the smallest strain step (1.3 $\mu\epsilon$) caused a measurable change in transmission. The resolution of this simple sensor was ~1 $\mu\epsilon$, which equals or exceeds that of considerably more complex (and expensive) sensor systems based on Bragg gratings.[5] The dynamic range was greater than 5000 $\mu\epsilon$. The resolution of the transmission measurements can be improved by use of an amplitude-stabilized light source and (or) a reference signal to normalize the transmission through the fiber. Key features of these real-time sensors are their simplicity and low cost; they do not require a spectrometer or time-consuming spectral processing. Also, because their grating resonance is broad, these sensors are relatively insensitive to drift in the wavelength of the light source.

We also demonstrated a temperature sensor by using the same grating. Temperature alters the refractive indices of the core and the cladding as well as the fiber geometry and so changes the coupling condition of a quadratic-dispersion grating. With a fixed strain, a change of temperature from 24 to 35 °C caused a change in transmission of 3%. Therefore, within the 0.01% resolution of our detector, we could resolve a 0.04 °C temperature change. We would improve the temperature sensitivity by an order of magnitude by doping the fiber core with boron.

Conventional sensor systems based on Bragg or conventional long-period fiber gratings rely on a change of resonant wavelength with temperature or strain. Consequently, such systems require an optical spectrum analyzer. Because scanning and analyzing the spectrum are required for each measurement, these systems can measure the parameter of interest only at discrete points of time.[5] Therefore systems based on a change of resonant wavelength are not well suited for high-speed or real-time applications.

In contrast, a quadratic-dispersion sensor works at a fixed wavelength. No spectrum analyzer is required. Using a light source at the resonant wavelength of the quadratic-dispersion grating and a simple photodetector, one can now perform measurements in real time. Because the resonance of a quadratic-dispersion grating is typically very broad (50–200 nm) and flat near its center, the light source need not be wavelength stabilized. An inexpensive LED would be well suited for this system. We also point out some disadvantages of this new sensor: its broad spectral width limits the number of such sensors that can be multiplexed on a single line, and it is sensitive to amplitude variations caused by bending of the lead fiber.

In conclusion, we have presented a new class of long-period grating—quadratic-dispersion gratings. Unlike in the common linear-dispersion long-period gratings, the resonance in a quadratic-dispersion long-period grating does not change its wavelength. Instead, its coupling strength changes with temperature or strain over a broad range. This new type of grating is well suited as a high-sensitivity sensor of strain or temperature (or other external factors), especially for real-time, low-cost applications.

J. Feinberg's e-mail address is feinberg@usc.edu.

References

1. A. M. Vengsarkar, P. L. Lemaire, J. B. Judkins, V. Bhatia, T. Erdogan, and J. E. Sipe, J. Lightwave Technol. **14,** 58 (1996).
2. V. Bhatia and A. M. Vengsarkar, Opt. Lett. **21,** 692 (1996).
3. X. Shu, X. Zhu, Q. Wang, S. Jiang, W. Shi, Z. Huang, and D. Huang, Electron. Lett. **35,** 649 (1999).
4. X. Shu, X. Zhu, Q. Wang, S. Jiang, W. Shi, and D. Huang, Electron. Lett. **35,** 1580 (1999).
5. A. D. Kersey, M. A. Davis, H. J. Patrick, M. LeBlanc, K. P. Poo, C. G. Askins, M. A. Putnam, and E. J. Friebele, J. Lightwave Technol. **15,** 1442 (1997).